Progress Report to

NATIONAL AERONAUTICS AND SPACE ADMINISTRATION
NASA Lewis Research Center

Grant NAG3-1273

HIGH-PERFORMANCE PARALLEL ANALYSIS OF COUPLED PROBLEMS FOR AIRCRAFT PROPULSION

by

C. A. FELIPPA, C. FARHAT, P.-S. CHEN,
U. GUMASTE, M. LESOINNE AND P. STERN

Department of Aerospace Engineering Sciences
and Center for Aerospace Structures
University of Colorado
Boulder, Colorado 80309-0429

February 1995

Report No. CU-CAS-95-03

Progress Report on Grant NAG3-1273 covering period from June 1994 through January 1995. This research is funded by NASA Lewis Research Center, 21000 Brookhaven Rd, Cleveland, Ohio 44135. Technical monitor: Dr. C. C. Chamis.

SUMMARY

This research program deals with the application of high-performance computing methods to the numerical simulation of complete jet engines. The program was initiated in 1993 by applying two-dimensional parallel aeroelastic codes to the interior gas flow problem of a by-pass jet engine. The fluid mesh generation, domain decomposition and solution capabilities were successfully tested. Attention was then focused on methodology for the partitioned analysis of the interaction of the gas flow with a flexible structure and with the fluid mesh motion driven by these structural displacements. The latter is treated by a ALE technique that models the fluid mesh motion as that of a fictitious mechanical network laid along the edges of near-field fluid elements. New partitioned analysis procedures to treat this coupled 3-component problem were developed in 1994. These procedures involved delayed corrections and subcycling, and have sucessfully tested on several massively parallel computers. For the global steady-state axisymmetric analysis of a complete engine we have decided to use the NASA-sponsored ENG10 program, which uses a regular FV-multiblock-grid discretization in conjunction with circumferential averaging to include effects of blade forces, loss, combustor heat addition, blockage, bleeds and convective mixing. A load-balancing preprocessor for parallel versions of ENG10 has been developed. It is planned to use the steady-state global solution provided by ENG10 as input to a localized three-dimensional FSI analysis for engine regions where aeroelastic effects may be important.

1. OVERVIEW

The present program deals with the application of high-performance parallel computation for the analysis of complete jet engines, considering the interaction of fluid, thermal and mechanical components. The research is driven by the simulation of advanced aircraft propulsion systems, which is a problem of primary interest to NASA Lewis.

The coupled problem involves interaction of structures with gas dynamics, heat conduction and heat transfer in aircraft engines. The *methodology* issues to be addressed include: consistent discrete formulation of coupled problems with emphasis on coupling phenomena; effect of partitioning strategies, augmentation and temporal solution procedures; sensitivity of response to problem parameters; and methods for interfacing multiscale discretizations. The *computer implementation* issues to be addressed include: parallel treatment of coupled systems; domain decomposition and mesh partitioning strategies; data representation in object-oriented form and mapping to hardware driven representation, and tradeoff studies between partitioning schemes with differing degree of coupling.

2. STAFF

Two graduate students were partly supported by this grant during 1994. M. Ronaghi (U.S. citizen) began his graduate studies at the University of Colorado on January 1993. He completed a M.Sc. in Aerospace Engineering on May 1994 and left to join Analytics Inc. (Hampton, VA) on June 1994.

U. Gumaste (permanent U.S. resident) began his graduate studies at Colorado in the Fall Semester 1993. Mr. Gumaste has a B.Tech in Civil Engineering from the Indian Institute of Technology, Bombay, India. He completed his Ph. D. course requirement in the Fall 1994 semester with the transfer of graduate credit units from the University of Maryland. On November 1994 he passed the Ph.D. Preliminary Exam thus becoming a doctoral candidate. During the Spring Semester 1994 he was partly supported as a Teaching Assistant. He familiarized himself with our aeroelastic codes in early summer 1994 and visited NASA Lewis for five weeks during July–August 1994.

One Post-Doctoral Research Associate, Paul Stern, was partly supported by this grant during the Spring Semester for running benchmarks on parallel computers. One graduate student, P.-S. Chen, supported by a related grant from NASA Langley, assisted with model preparation tasks.

The development of FSI methodology for this project has benefited from the presence of several visiting Post-Docs whose work concentrated on the related problem of exterior aeroelasticity for a complete aircraft. This project was part of a Grant Challenge Applications Award supported by NSF, but most aspects of the solution methodology and parallel implementation are applicable to FSI engine problems. Dr. S. Lanteri conducted extensive experimentation on several computational algorithms for compressive viscous flow simulation on the iPSC-860, CM-5 and KSR-1 as reported in the July 1994 Progress Report. Dr. N. Maman implemented "mesh matching" techniques that connect separately generated fluid and structural meshes. Dr. S. Piperno developed and evaluated implicit and subcycled partitioned analysis procedures for the interaction of structure, fluid and fluid-mesh motion. A new approach to augmentation of the governing semi-discrete equations that

improves stability while keeping communications overhead modest was investigated. Finally, Dr. M. Lesoinne (who finsished his Ph.D. under C. Farhat on August 1994 and is presently a Research Associate) made significant contributions to the modeling and computational treatment of the fluid mesh motion, and the development of global conservation laws that must be obeyed by those motions.

Preliminary results from these studies were presented in the July 1994 Progress Report. The first 3D aeroelastic parallel calculations undertaken with these methods are reported in Appendix I of the present report.

3. DEVELOPMENT OF PARTITIONED ANALYSIS METHODS

The first parallel computations of a jet engine, presented in the first Progress Report, dealt with the fluid flow within a jet engine structure that is considered rigid and hence provides only guiding boundary conditions for the gas flow. When the structural flexibility is accounted for two complications occur:

1. The engine simulation algorithm must account for the structural flexibility though periodic transfer of interaction information, and
2. The fluid mesh must smoothly follow the relative structural motions through an ALE (Adaptive Lagrangian Eulerian) scheme. The particular ALE scheme selected for the present work makes use of Batina's proposed pseudo-mechanical model of springs and masses overlaid over the fluid mesh.

Research work during the period July 1993 through January 1994 was dominated by the treatment of two subjects: partitioned analysis of fluid-structure interaction (FSI) and accounting for fluid mesh motions. The partitioned analysis algorithm developed for the FSI problem is always implicit in the structure (because of its larger time scale of significant vibratory motions) and either explicit or implicit for the gas flow modeled by the Navier-Stokes equations. Subcycling, in which the integration stepsize for the fluid may be smaller than that used in the structure, was also studied.

3.1. General Requirements

The fundamental practical considerations in the development of these methods are: (1) numerical stability, (2) fidelity to physics, (3) accuracy, and (4) MPP efficiency. Numerical stability is fundamental in that an unstable method, no matter how efficient, is useless. There are additional considerations:

1. Stability degradation with respect to that achievable for the *uncoupled* fields should be minimized. For example, if the treatment is implicit-implicit (I-I) we would like to maintain unconditional stability. If the fluid is treated explicitly we would like to maintain the same CFL stability limit.
2. Masking of physical instability should be avoided. This is important in that flutter or divergence phenomena should not be concealed by numerical dissipation. For this reasons all time integration algorithms considered in this work must exclude the use of artificial damping.

3.2. Stability vs. Communication-Overhead Tradeoff

The degradation of numerical stability degradation is primarily influenced by the nature of information exchanged every time step among the coupled subsystems during the course of partitioned integration. A methodology called *augmentation* that systematically exploits this idea was developed by Park and Felippa in the late 1970s. The idea is to modify the governing equations of one subsystem with system information from connected subsystems. The idea proved highly successful for the sequential computers of the time. A fresh look must be taken to augmentation, however, in light of the communications overhead incurred in massively parallel processing. For the present application three possibilities were considered:

No augmentation. The 3 subsystems (fluid, structure and ALE mesh) exchange only minimal interaction state information such as pressures and surface-motion velocities, but no information on system characteristics such as mass or stiffness. The resulting algorithm has minimal MPP communication overhead but poor stability characteristics. In fact the stability of an implicit-implicit scheme becomes conditional and not too different from that of a less expensive implicit-explicit scheme. This degradation in turn can significantly limit the stepsize for both fluid and structure.

Full augmentation. This involves transmission of inverse-matrix-type data from one system to another. Such data are typified by terms such as a a structure-to-fluid coupling-matrix times the inverse of the structural mass. Stability degradation can be reduced or entirely eliminated; for example implicit-implicit unconditional stability may be maintained. But because the transmitted matrix combinations tend to be much less sparse than the original system matrices, the MPP communications overhead can become overwhelming, thus negating the benefits of improved stability characteristics.

Partial augmentation. This new approach involves the transmission of coupling matrix information which does not involve inverses. It is efficiently implemented as a delayed correction to the integration algorithm by terms proportional to the squared stepsize. The MPP communication requirements are modest in comparison to the fully-augmented case, whereas stability degradation can be again eliminated with some additional care.

The partial augmentation scheme was jointly developed by S. Piperno and C. Farhat in early 1994. Its derivation is reported in Appendix I of the July 1994 report. This work has been submitted and accepted for publication in referred journals.

The use of these methods in three-dimensional aeroelasticity has been investigated from the summer 1994 to the present time. This investigation has resulted in the development of four specific algorithms for explicit/implicit staggered time integration, which are labeled as A0 through A4. The basic algorithm A0 is suitable for sequential computers when the time scale and computational cost of fluid and structure components is comparable. Algorithm A1 incorporates fluid subcycling. Algorithms A2 and A3 aim to exploit inter-field parallelism by allowing the integration over fluid and structure to proceed concurrently, with A3 aimed at achieving better accuracy through a more complex field synchronization scheme. These algorithms are described in more detail in Appendix I of this report.

3.3. Effects of Moving Fluid Mesh

The first one-dimensional results on the effect of a dynamic fluid mesh on the stability and accuracy of the staggered integration were obtained by C. Farhat and S. Piperno in late 1993 and early 1994, and are discussed in Appendix II of the July 1994 report. A doctoral student, M. Lesoinne (presently a post-doctoral Research Associate supported by a related NSF grant) extended those calculations to the multidimensional case. This work culminated in the development of a geometric conservation law (GCL) that must be verified by the mesh motion in the three-dimensional case. This law applies to unstructured meshes typical of finite element and finite-volume fluid discretizations, and extends the GCL enunciated for regular finite-difference discretizations by Thomas and Lombard in 1977. This new result is presented in more detail in Appendix I of this report.

3.4. Benchmarking on Parallel Computers

The new staggered solution algorithms for FSI, in conjunction with the improved treatment of fluid mesh motion dictated by the GCL, have been tested on several massively-parallel computational platforms using benchmark aerodynamic and FSI problems. These platforms include the Intel i860 Hypercube, Intel XP/S Paragon, Cray T3D, and IBM SP2. Performance results from these tests are reported and discussed in Appendix I of this report.

4. MODELING OF COMPLETE ENGINE

Work on the global model of a complete engine proceeded through two phases during 1994.

4.1. Homogenized Modeling of Compressor and Combustion Areas

Initial work in this topic in the period 1/94 through 4/94 was carried out using "energy injection" ideas. This idea contemplated feeding (or removing) kinetic and thermal energy into fluid mesh volume elements using the total-energy variables as "volume forcing" functions.

Although promising, energy injection in selected blocks of fluid volumes was found to cause significant numerical stability difficulties in the transient gas-flow analysis, which used explicit time integration. Consequently the development of these methods was put on hold because of the decision to use the program `ENG10` (which is briefly described in 4.2 below) for flow global analysis. `ENG10` makes use of similar ideas but the formulation of the governing equations and source terms in a rotating coordinate system is different. In addition a semi-implicit multigrid method, rather than explicit integration, is used to drive the gas flow solution to the steady state condition, resulting in better stability characteristics.

4.2. Load Balancing Preprocessor for Program `ENG10`

As a result of Mr. Gumaste's visit to NASA Lewis during July-August of 1994, it was decided to focus on the `ENG10` code written by Dr. Mark Stewart of NYMA Research Corp. to carry out the parallel analysis of a complete engine. This program was developed under contract with NASA Lewis, the contract monitors of this project being Austin Evans and Russell Claus.

ENG10 is a research program designed to carry out a "2 1/2" dimensional" flow analysis of a complete turbofan engine taking into account — through appropriate circumferential averaging — blade forces, loss, combustor heat addition, blockage, bleeds and convective mixing. The engine equations are derived from the three-dimensional fluid flow equations in a rotating cylindrical coordinate system. The Euler fluid flow equations express conservation of mass, momentum and rothalpy. These equations are discretized by structured finite-volume (FV) methods. The resulting discrete model is treated by multiblock-multigrid solution techniques. A multiblock grid divides the computational domain into topologically rectangular blocks in each of which the grid is regular (structured). For bladed jet engine geometries, this division is achieved through a series of supporting programs, namely TOPOS, TF and MS.

During the period September through December 1994, Mr. Gumaste devoted his time to the following tasks.

(a) Understanding the inner workings of ENG10 and learning to prepare inputs to this program (for which there is no user manual documentation) with the assistance from Dr. Stewart.

(b) Provide for links to the pre/postprocessor TOPS/DOMDEC developed by Charbel Farhat's group to view the decomposed model and analysis results.

(c) Develop and test algorithms for load-balancing the aerodynamic analysis of ENG10 in anticipation of running that program on parallel computers. The algorithm involves iterative merging and splitting of original blocks while respecting grid regularity constraints. This development resulted in a Load-Balancing (LB) program that can be used to adjust the original multiblock-grid discretization before starting ENG10 analysis runs on remote parallel computers (or local workstation networks).

Subtasks (b) and (c) were tested on a General Electric Energy Efficient Engine (GE-EEE) model provided by Dr. Stewart. A report on the development of LB is provided in Appendix II of this report.

5. NEAR-TERM WORK

For the performance period through September1995 it was decided, upon consultation with the Grant Technical Monitor, to pursue the idea of using the ENG10 program to produce global flow-analysis results that can be subsequently used as inputs for 3D aeroelastic analysis of selected engine regions. This embodies the first two Tasks (5.1 and 5.2) presented below. Task 5.3 depends on timely availability of a parallelized version of ENG10 and would not affect work in the more important Tasks 5.1 and 5.2.

5.1. Global-Local Data Transfer

This involves the ability to extract converged axisymmetric solutions from ENG10 and convert to entry exit boundary for the TOP/DOMDEC 3D aeroelastic analyzer PARFSI. This fluid model used by this program is based on the full Navier Stokes equations and includes a wall turbulence model. It is hence well suited for capturing local effects such as shocks and interferences.

5.2. Blade Flutter Analysis

This involving carrying out the time-domain transonic flutter analysis of a typical turbine blade using global-local techniques. The finite element model of the blade is to be constructed by Mr. Gumaste and verified during his summer visit to NASA LeRC, in consultation with an aeroelasticity specialist.

Because the input conditions provided by `ENG10` are of steady state type, flutter may be tested by imposing initial displacement perturbations on the blade and tracing its time response. Additional information that may be provided by this detailed analysis is feedback into possible physics limitations of the axisymmetric global model by noting the appearance of microscale effects (e.g., shocks) and deviations from the steady state exit conditions.

Conceivable this local model may include several blades using sector-symmetry generators. The analysis is to be carried out using the TOP/DOMDEC aeroelastic analyzer PARFSI on the Cray T3D or IBM SP2 computers.

5.3. Paralellized `ENG10` benchmarking

Dr. Stewart has kindly offered to provide us a parallelized version of `ENG10` presently being developed under contract with NASA LeRC. If this version is available before the summer, `ENG10` would be run on a MIMD machine such as a Cray T3D or IBM SP2 with varying number of processors to assess scalability and load balance. Results may be compared to those obtained by the PARFSI aeroelastic analyzer for a similar number of degrees of freedom in the fluid volume.

Appendix I

Parallel Staggered Algorithms for the Solution of Three-Dimensional Aeroelastic Problems

Summary

This Appendix outlines recent developments in the solution of large-scale three-dimensional (3D) nonlinear aeroelastic problems on high performance, massively-parallel computational platforms. Developments include a three-field arbitrary Lagrangian-Eulerian (ALE) finite volume/element formulation for the coupled fluid/structure problem, a geometric conservation law for 3D flow problems with moving boundaries and unstructured deformable meshes, and the solution of the corresponding coupled semi-discrete equations with partitioned heterogeneous procedures. We present a family of mixed explicit/implicit staggered solution algorithms, and discuss them with particular reference to accuracy, stability, subcycling, and parallel processing. We describe a general framework for the solution of coupled aeroelastic problems on heterogeneous and/or parallel computational platforms, and illustrate it with some preliminary numerical investigations of transonic aerodynamics and aeroelastic responses on several massively parallel computers, including the iPSC-860, Paragon XP/S, Cray T3D, and IBM SP2. The work described here was carried out by P.-S. Chen, M. Lesoinne and P. Stern under supervision from Professor C. Farhat.

I.1. INTRODUCTION

In order to predict the aeroelastic behavior of flexible structures in fluid flows, the equations of motion of the structure and the fluid must be solved simultaneously. Because the position of the structure determines at least partially the boundaries of the fluid domain, it becomes necessary to perform the integration of the fluid equations on a moving mesh. Several methods have been proposed for this purpose. Among them we note the Arbitrary Lagrangian Eulerian (ALE) formulation [7], dynamic meshes [3], the co-rotational approach [8,11,22], and the Space-Time finite element method [39].

Although the aeroelastic problem is usually viewed as a two-field coupled problem (see for example, Guruswamy [20]), the moving mesh can be viewed as a pseudo-structural system with its own

dynamics, and therefore, the coupled aeroelastic system can be formulated as a three-field problem, the components of which are the fluid, the structure, and the dynamic mesh [24]. The semi-discrete equations that govern this three-way coupled problem can be written as follows.

$$\boxed{\begin{aligned} \frac{\partial}{\partial t}(\mathbf{V}(\mathbf{x},t)\,\mathbf{w}(t)) + \mathbf{F}^c(\mathbf{w}(t),\mathbf{x},\dot{\mathbf{x}}) &= \mathbf{R}(\mathbf{w}(t)) \\ \mathbf{M}\frac{\partial^2 \mathbf{q}}{\partial t^2} + \mathbf{f}^{int}(\mathbf{q}) &= \mathbf{f}^{ext}(\mathbf{w}(t),\mathbf{x}) \\ \widetilde{\mathbf{M}}\frac{\partial^2 \mathbf{x}}{\partial t^2} + \widetilde{\mathbf{D}}\frac{\partial \mathbf{x}}{\partial t} + \widetilde{\mathbf{K}}\mathbf{x} &= \mathbf{K}_c\,\mathbf{q} \end{aligned}} \tag{1}$$

where t denotes time, $\mathbf{x}$ is the position of a moving fluid grid point, $\mathbf{w}$ is the fluid state vector, $\mathbf{V}$ results from the flux-split finite-element (FE) and finite-volume (FV) discretization of the fluid equations, $\mathbf{F}^c$ is the vector of convective ALE fluxes, $\mathbf{R}$ is the vector of diffusives fluxes, $\mathbf{q}$ is the structural displacement vector, $\mathbf{f}^{int}$ denotes the vector of internal forces in the structure, $\mathbf{f}^{ext}$ the vector of external forces, $\mathbf{M}$ is the FE mass matrix of the structure, $\widetilde{\mathbf{M}}$, $\widetilde{\mathbf{D}}$ and $\widetilde{\mathbf{K}}$ are fictitious mass, damping and stiffness matrices associated with the moving fluid grid, and $\mathbf{K}_c$ is a transfer matrix that describes the action of the motion of the structural side of the fluid/structure interface on the fluid dynamic mesh.

For example, $\widetilde{\mathbf{M}} = \widetilde{\mathbf{D}} = 0$, and $\widetilde{\mathbf{K}} = \widetilde{\mathbf{K}}^R$ where $\widetilde{\mathbf{K}}^R$ is a rotation matrix corresponds to a rigid mesh motion of the fluid grid around an oscillating airfoil, and $\widetilde{\mathbf{M}} = \widetilde{\mathbf{D}} = 0$ includes as particular cases the spring-based mesh motion scheme introduced by Batina [3], and the continuum based updating strategy described by Tezduyar [39]. In general, $\mathbf{K}^c$ and $\tilde{\mathbf{K}}$ are designed to enforce continuity between the motion of the fluid mesh and the structural displacement and/or velocity at the fluid/structure boundary $\Gamma_{F/S}(t)$:

$$\begin{aligned} x(t) &= q(t) \quad \text{on } \Gamma_{F/S}(t) \\ \dot{x}(t) &= \dot{q}(t) \quad \text{on } \Gamma_{F/S}(t) \end{aligned} \tag{2}$$

Each of the three components of the coupled problem described by Eqs. (1) has different mathematical and numerical properties, and distinct software implementation requirements. For Euler and Navier-Stokes flows, the fluid equations are nonlinear. The structural equations and the semi-discrete equations governing the pseudo-structural fluid grid system may be linear or nonlinear. The matrices resulting from a linearization procedure are in general symmetric for the structural problem, but they are typically unsymmetric for the fluid problem. Moreover, the nature of the coupling in Eqs. (1) is implicit rather than explicit, even when the fluid mesh motion is ignored. The fluid and the structure interact only at their interface, via the pressure and the motion of the physical interface. However, for Euler and Navier-Stokes compressible flows, the pressure variable cannot be easily isolated neither from the fluid equations nor from the fluid state vector $\mathbf{w}$. Consequently, the numerical solution of Eqs. (1) via a fully coupled monolithic scheme is not only computationally challenging, but unwieldy from the standpoint of software development management.

Alternatively, Eqs. (1) can be solved via partitioned procedures [4,9,30], the simplest realization of which are the staggered procedures [29]. This approach offers several appealing features, including the ability to use well established discretization and solution methods within each discipline, simplification of software development efforts, and preservation of software modularity. Traditionally, transient aeroelastic problems have been solved via the simplest possible staggered procedure whose typical cycle can be described as follows: a) advance the structural system under a given pressure load, b) update the fluid mesh accordingly, and c) advance the fluid system and compute a new pressure load [5,6,33,34]. Some investigators have advocated the introduction of a few predictor/corrector iterations within each cycle of this three-step staggered integrator in order to improve accuracy [38], especially when the fluid equations are nonlinear and treated implicitly [32]. Here we focus on the design of a broader family of partitioned procedures where the fluid flow is integrated using an explicit scheme, and the structural response is advanced using an implicit one. We address issues pertaining to numerical stability, subcycling, accuracy v.s. speed trade-offs, implementation on heterogeneous computing platforms, and inter-field as well as intra-field parallel processing.

We begin in Section I.2 with the discussion of a geometric conservation law (GCL) for the finite-volume approximation of three-dimensional flows with moving boundaries. In Section I.3 we introduce a partitioned solution procedure where the fluid flow is time-integrated using an explicit scheme while the structural response is advanced using an implicit scheme. This particular choice of mixed time-integration is motivated by the following facts: (a) the aeroelastic response of a structure is often dominated by low frequency dynamics, and therefore is most efficiently predicted by an implicit time-integration scheme, and (b) we have previously developed a massively parallel explicit FE/FV Navier-Stokes solver that we wish to re-use for aeroelastic computations. Two-dimensional versions of this solver have been described by Farhat and coworkers [10,12,23].

In practice, the stability limit of this partitioned procedure has proved to be governed only by the critical time-step of the explicit fluid solver. In Section II.4, we describe a subcycling procedure that does not limit the stability properties of a partitioned time-integrator. In Section I.5, we address important issues related to inter-field parallelism and design variants of the algorithm presented in Section I.3 that allow advancing simultaneously the fluid and structural systems. Section I.6 focuses on the implementation of staggered procedures on distributed and/or heterogeneous computational platforms. Finally, Section I.7 illustrates the work presented herein with some preliminary numerical results on four parallel computers: Intel iPSC-860, Intel Paragon XP/S, Cray T3D, and IBM SP2. These results pertain to the response of an axisymmetric engine model and of a 3D wing in a transonic airstream.

I.2. A GLOBAL CONSERVATION LAW FOR ALE-BASED FV METHODS

I.2.1. Semi-discrete flow equations

Let $\Omega(t) \subset \mathcal{R}^3$ be the flow domain of interest, and $\Gamma(t)$ be its moving and deforming boundary. For simplicity, we map the instantaneous deformed domain on the reference domain $\Omega(0)$ as follows:

$$x = x(\xi, t), \qquad t = \tau \tag{3}$$

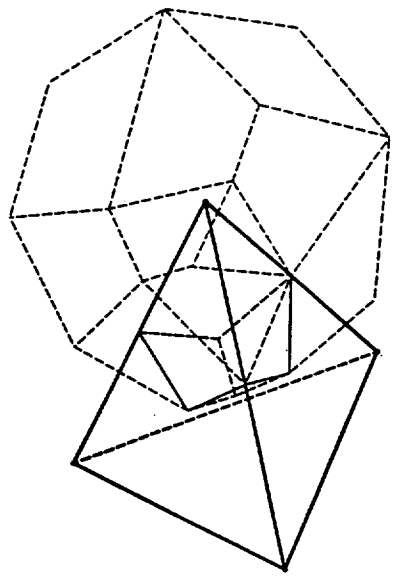

Figure I.1. A three-dimensional unstructured FV cell

The ALE conservative form of the equations describing Euler flows can be written as:

$$\left.\frac{\partial(JW)}{\partial t}\right|_{\xi} + J\nabla_x.\mathcal{F}^c(W) = 0, \qquad \mathcal{F}^c(W) = \mathcal{F}(W) - \dot{x}W \tag{4}$$

where $J = \det(dx/d\xi)$ is the Jacobian of the frame transformation $\xi \rightarrow x$, W is the fluid state vector, $\mathcal{F}^c$ denotes the convective ALE fluxes, and $\dot{x} = \frac{\partial x}{\partial \tau}|_{\xi}$ is the ALE grid velocity, which may be different from the fluid velocity and from zero. The fluid volume method for unstructured meshes relies on the discretization of the computational domain into control volumes or cells C_i, as illustrated in Fig. I.1.

Because in an ALE formulation the cells move and deform in time, the integration of Eq. (4) is first performed over the reference cell in the ξ space

$$\int_{C_i(0)} \left.\frac{\partial(JW)}{\partial t}\right|_{\xi} d\Omega_{\xi} + \int_{C_i(0)} J\nabla_x.\mathcal{F}^c(W)\, d\Omega_{\xi} = 0 \tag{5}$$

Note that in Eq. (5) above the time derivative is evaluated at a constant ξ; hence it can be moved outside of the integral sign to obtain

$$\frac{d}{dt}\int_{C_i(0)} W\, J\, d\Omega_{\xi} + \int_{C_i(0)} \nabla_x.\mathcal{F}^c(W)\, J\, d\Omega_{\xi} = 0 \tag{6}$$

Switching back to the time varying cells, we have

$$\frac{d}{dt}\int_{C_i(t)} W\, d\Omega_x + \int_{C_i(t)} \nabla_x.\mathcal{F}^c(W)\, d\Omega_x = 0 \tag{7}$$

Finally, integrating by parts the last term yields the integral equation

$$\frac{d}{dt}\int_{C_i(t)} W\, d\Omega_x + \int_{\partial C_i(t)} \mathcal{F}^c(W).\vec{n}\, d\sigma = 0 \tag{8}$$

A key component of a FV method is the following approximation of the flux through the cell boundary $\partial C_i(t)$:

$$F_i(\mathbf{w}, \mathbf{x}, \dot{\mathbf{x}}) = \sum_j \int_{\partial C_{i,j}(\mathbf{x})} (\mathcal{F}^c_+(W_i, \dot{x}) + \mathcal{F}^c_-(W_j, \dot{x}))\, \vec{n}\, d\sigma \tag{9}$$

where W_i denotes the average value of W over the cell C_i, $\mathbf{w}$ is the vector formed by the collection of W_i, and $\mathbf{x}$ is the vector of time dependent nodal positions. The numerical flux functions $\mathcal{F}^c_+$ and $\mathcal{F}^c_-$ are designed to make the resulting system stable. An example of such functions may be found in Ref. [1]. For consistency, these numerical fluxes must verify

$$\mathcal{F}^c_+(W, \dot{x}) + \mathcal{F}^c_-(W, \dot{x}) = \mathcal{F}^c(W) \tag{10}$$

Thus, the governing discrete equation is:

$$\frac{d}{dt}(V_i W_i) + F_i(\mathbf{w}, \mathbf{x}, \dot{\mathbf{x}}) = 0 \tag{11}$$

where

$$V_i = \int_{C_i(t)} d\Omega_x \tag{12}$$

is the volume of cell C_i. Collecting all Eqs. (11) into a single system yields:

$$\frac{d}{dt}(\mathbf{V}\mathbf{w}) + \mathbf{F}(\mathbf{w}, \mathbf{x}, \dot{\mathbf{x}}) = 0 \tag{13}$$

where $\mathbf{V}$ is the diagonal matrix of the cell volumes, $\mathbf{w}$ is the vector containing all state variables W_i, and $\mathbf{F}$ is the collection of the ALE fluxes F_i.

I.2.2. A Geometric Conservation Law

Let Δt and $t^n = n\Delta t$ denote the chosen time-step and the n-th time-station, respectively. Integrating Eq. (11) between t^n and t^{n+1} leads to

$$\begin{aligned}\int_{t^n}^{t^{n+1}} \frac{d}{dt}(V_i(\mathbf{x}) W_i) dt + \int_{t^n}^{t^{n+1}} & F_i(\mathbf{w}, \mathbf{x}, \dot{\mathbf{x}}) \\ &= V_i(\mathbf{x}^{n+1}) W_i^{n+1} - V_i(\mathbf{x}^n) W_i^n \\ &+ \int_{t^n}^{t^{n+1}} F_i(\mathbf{w}, \mathbf{x}, \dot{\mathbf{x}}) = 0\end{aligned} \tag{14}$$

The most important issue in the solution of the first of Eqs. (1) via an ALE method is the proper evaluation of $\int_{t^n}^{t^{n+1}} F_i(\mathbf{w}, \mathbf{x}, \dot{\mathbf{x}})$ in Eq. (14). In particular, it is crucial to establish where the fluxes must be integrated: on the mesh configuration at $t = t^n(\mathbf{x}^n)$, on the configuration at $t = t^{n+1}(\mathbf{x}^{n+1})$, or in between these two configurations. The same questions also arise as to the choice of the mesh velocity vector $\dot{\mathbf{x}}$.

Let W^* denote a given uniform state of the flow. Clearly, a proposed solution method cannot be acceptable unless it conserves the state of a uniform flow. Substituting $W_k^n = W_k^{n+1} = W^*$ in Eq. (14) gives:

$$(V_i^{n+1} - V_i^n)W^* + \int_{t^n}^{t^{n+1}} F_i(\mathbf{w}^*, \mathbf{x}, \dot{\mathbf{x}})\, dt = 0 \tag{15}$$

in which $\mathbf{w}^*$ is the vector of the state variables when $W_k = W^*$ for all k. From Eq. (9) it follows that:

$$F_i(\mathbf{w}^*, \mathbf{x}, \dot{\mathbf{x}}) = \int_{\partial C_i(\mathbf{X})} (\mathcal{F}(W^*) - \dot{x}W^*)\, d\sigma \tag{16}$$

Given that the integral on a closed boundary of the flux of a constant function is identically zero we must have

$$\int_{\partial C_i(\mathbf{X})} \mathcal{F}(W^*)\, d\sigma = 0 \tag{17}$$

it follows that

$$F_i(\mathbf{w}^*, \mathbf{x}, \dot{\mathbf{x}}) = -\int_{\partial C_i(\mathbf{X})} \dot{x}W^*\, d\sigma \tag{18}$$

Hence, substituting Eq. (18) into Eq. (15) yields

$$(V_i(\mathbf{x}^{n+1}) - V_i(\mathbf{x}^n))W^* - (\int_{t^n}^{t^{n+1}} \int_{\partial C_i(\mathbf{X})} \dot{x}\, d\sigma\, dt)W^* = 0 \tag{19}$$

which can be rewritten as

$$\boxed{(V_i(\mathbf{x}^{n+1}) - V_i(\mathbf{x}^n)) = \int_{t^n}^{t^{n+1}} \int_{\partial C_i(\mathbf{X})} \dot{x}\, d\sigma\, dt} \tag{20}$$

Eq. (20) must be verified by any proposed ALE mesh updating scheme. We refer to this equation as the geometric conservation law (GCL) because: (a) it can be identified as integrating exactly the volume swept by the boundary of a cell in a FV formulation, (b) its principle is similar to the GCL condition that was first pointed out by Thomas and Lombard [40] for structured grids treated by finite difference schemes. More specifically, this law states that the change in volume of each cell between t^n and t^{n+1} must be equal to the volume swept by the cell boundary during the time-step $\Delta t = t^{n+1} - t^n$. Therefore, the updating of $\mathbf{x}$ and $\dot{\mathbf{x}}$ cannot be based on mesh distorsion issues alone when using ALE solution schemes.

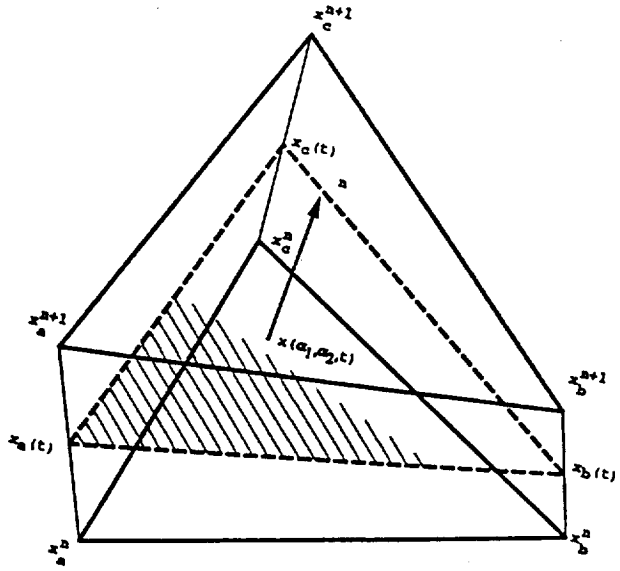

Figure I.2. Parametrization of a moving triangular facet.

I.2.3. Implications of the Geometric Conservation Law

From the analysis presented in the previous section, it follows that an appropriate scheme for evaluating $\int_{t^n}^{t^{n+1}} F_i(\mathbf{w}^*, \mathbf{x}, \dot{\mathbf{x}})dt$ is a scheme that respects the GCL condition (20). Note that once a mesh updating scheme is given, the left hand side of Eq. (20) can be always computed. Hence, a proper method for evaluating $\int_{t^n}^{t^{n+1}} F_i(\mathbf{w}^*, \mathbf{x}, \dot{\mathbf{x}})dt$ is one that obeys the GCL and therefore computes exactly the right hand side of Eq. (20) — that is, $\int_{t^n}^{t^{n+1}} \int_{\partial C_i(\mathbf{X})} \dot{x}\, d\sigma\, dt$.

In three-dimensional space each tetrahedral cell is bounded by a collection of triangular facets. Let $I_{[abc]}$ denote the mesh velocity flux crossing a facet $[abc]$:

$$I_{[abc]} = \int_{t^n}^{t^{n+1}} \int_{[abc]} \dot{x}.\vec{n}\, d\sigma dt \tag{21}$$

and let x_a, x_b and x_c denote the instantaneous positions of the three connected vertices a, b and c. The position of any point on the facet can be parametrized as follows (see Figure I.2)

$$\begin{aligned} x &= \alpha_1 \mathbf{x}_a(t) + \alpha_2 \mathbf{x}_b(t) + (1 - \alpha_1 - \alpha_2)\mathbf{x}_c(t) \\ \dot{x} &= \alpha_1 \dot{\mathbf{x}}_a(t) + \alpha_2 \dot{\mathbf{x}}_b(t) + (1 - \alpha_1 - \alpha_2)\dot{\mathbf{x}}_c(t) \\ \alpha_1 &\in [0,\ 1];\quad \alpha_2 \in [0,\ 1 - \alpha_1];\quad t \in [t^n,\ t^{n+1}] \end{aligned} \tag{22}$$

where

$$x_i(t) \ = \ \delta(t)x_i^{n+1} + (1 - \delta(t))x_i^n \quad i = a,\ b,\ c \tag{23}$$

and $\delta(t)$ is a real function satisfying

$$\delta(t^n) = 0; \quad \delta(t^{n+1}) = 1 \tag{24}$$

Substituting the above parametrization in Eq. (21) leads to

$$I_{[abc]} = \int_0^1 \frac{1}{3}(\Delta x_a + \Delta x_b + \Delta x_c).(x_{ac} \wedge x_{bc})\, d\delta \tag{25}$$

where

$$\begin{aligned} x_{ac} = x_a - x_c; \quad x_{bc} = x_b - x_c; \quad \Delta x_a = x_a^{n+1} - x_a^n \\ \Delta x_b = x_b^{n+1} - x_b^n; \quad \Delta x_c = x_c^{n+1} - x_c^n \end{aligned} \tag{26}$$

and the mesh velocities $\dot{x}_a$, $\dot{x}_b$ and $\dot{x}_c$ are obtained from the differentiation of Eqs. (23):

$$\dot{x}_a = \dot{\delta}(t)(x_a^{n+1} - x_a^n) \quad i = a,\ b,\ c \tag{27}$$

Finally, noting that

$$x_{ac} \wedge x_{bc} = \left((\delta x_{ac}^{n+1} + (1-\delta)x_{ac}^n) \wedge (\delta x_{bc}^{n+1} + (1-\delta)x_{bc}^n)\right) \tag{28}$$

is a quadratic function of δ, it becomes clear that the integrand of $I_{[abc]}$ is quadratic in δ, and therefore can be exactly computed using a *two-point integration rule*, provided that Eqs. (27) hold. That is,

$$\dot{x} = \dot{\delta}(t)(x^{n+1} - x^n) = \frac{\Delta\delta}{\Delta t}(x^{n+1} - x^n) \tag{29}$$

which in view of Eq. (24) can also be written as:

$$\boxed{\dot{x} = \frac{x^{n+1} - x^n}{\Delta t}} \tag{30}$$

Summarizing, an appropriate method for evaluating $\int_{t^n}^{t^{n+1}} F_i(\mathbf{w}, \mathbf{x}, \dot{\mathbf{x}})\, dt$ that respects the GCL condition (20) is

$$\boxed{\begin{aligned} \int_{t^n}^{t^{n+1}} F_i(\mathbf{w}, \mathbf{x}, \dot{\mathbf{x}})\, dt &= \frac{\Delta t}{2}(F_i(\mathbf{w}^n, \mathbf{x}^{m1}, \dot{\mathbf{x}}^{n+\frac{1}{2}}) \\ &\quad + F_i(\mathbf{w}^n, \mathbf{x}^{m2}, \dot{\mathbf{x}}^{n+\frac{1}{2}})) \\ m1 &= n + \frac{1}{2} + \frac{1}{2\sqrt{3}} \\ m2 &= n + \frac{1}{2} - \frac{1}{2\sqrt{3}} \\ \mathbf{w}^{n+\eta} &= \eta\mathbf{w}^{n+1} + (1-\eta)\mathbf{w}^n \\ \mathbf{x}^{n+\eta} &= \eta\mathbf{x}^{n+1} + (1-\eta)\mathbf{x}^n \\ \dot{\mathbf{x}}^{n+\frac{1}{2}} &= \frac{\mathbf{x}^{n+1} - \mathbf{x}^n}{2} \end{aligned}} \tag{31}$$

I.3. A STAGGERED EXPLICIT/IMPLICIT TIME INTEGRATOR

I.3.1. Background

When the structure undergoes small displacements, the fluid mesh can be frozen and "transpiration" fluxes can be introduced at the fluid side of the fluid/structure boundary to account for the motion of the structure. In that case, the transient aeroelastic problem is simplified from a three- to a two-field coupled problem.

Furthermore, if the structure is assumed to remain in the linear regime and the fluid flow is linearized around an equilibrium position W_0 (note that most fluid/structure instability problems are analyzed by investigating the response of the coupled system to a perturbation around a steady state), the semi-discrete equations governing the coupled aeroelastic problem become (see [31] for details):

$$\begin{aligned} \begin{bmatrix} \dot{\delta \mathbf{w}} \\ \dot{\mathbf{s}} \end{bmatrix} &= \begin{bmatrix} \mathbf{A} & \mathbf{B} \\ \mathbf{C} & \mathbf{E} \end{bmatrix} \begin{pmatrix} \delta \mathbf{w} \\ \mathbf{s} \end{pmatrix} \\ \begin{bmatrix} \delta \mathbf{w} \\ \mathbf{s} \end{bmatrix}_{(t=0)} &= \begin{bmatrix} \delta \mathbf{w} \\ \mathbf{s} \end{bmatrix}_0 \end{aligned} \tag{32}$$

where $\delta \mathbf{w}$ is the perturbed fluid state vector, $\mathbf{s} = \begin{pmatrix} \mathbf{q} \\ \dot{\mathbf{q}} \end{pmatrix}$ is the structure state vector, matrix $\mathbf{A}$ results from the spatial discretization of the flow equations, $\mathbf{B}$ is the matrix induced by the transpiration fluxes at the fluid/structure boundary $\Gamma_{F/S}$, $\mathbf{C}$ is the matrix that transforms the fluid pressure on $\Gamma_{F/S}$ into prescribed structural forces; finally $\mathbf{E} = \begin{bmatrix} \mathbf{O} & \mathbf{I} \\ -\mathbf{M}^{-1}\mathbf{K} & -\mathbf{M}^{-1}\mathbf{D} \end{bmatrix}$, where $\mathbf{M}$, $\mathbf{D}$, and $\mathbf{K}$ are the structural mass, damping, and stiffness matrices.

A mathematical discussion of the time-integration of Eqs. (32) via implicit/implicit and explicit/implicit partitioned procedures can be found in Ref. [31]. In the present work we focus on the more general three-way coupled aeroelastic problem (1). Based on the mathematical results established in [12] for solving Eqs. (32), we design a family of explicit/implicit staggered procedures for time-integrating Eqs. (1), and address important issues pertaining to accuracy, stability, distributed computing, subcycling, and parallel processing.

I.3.2. A0: An Explicit/Implicit Algorithm

We consider 3D nonlinear Euler flows and linear structural vibrations. From the results established in Section I.2, it follows that the semi-discrete equations governing the three-way coupled aeroelastic problem can be written as:

$$
\begin{aligned}
&\mathbf{V}(\mathbf{x}^{n+1})\mathbf{w}^{n+1} - \mathbf{V}(\mathbf{x}^{n})\mathbf{w}^{n} \\
&\qquad + \frac{\Delta t}{2}(\mathbf{F}^{c}(\mathbf{w}^{n},\ \mathbf{x}^{m1},\ \dot{\mathbf{x}}^{n+\frac{1}{2}}) \\
&\qquad + \mathbf{F}^{c}(\mathbf{w}^{n},\ \mathbf{x}^{m2},\ \dot{\mathbf{x}}^{n+\frac{1}{2}})) \ = \ 0 \\
&m1 = n + \frac{1}{2} + \frac{1}{2\sqrt{3}} \\
&m2 = n + \frac{1}{2} - \frac{1}{2\sqrt{3}} \\
&\mathbf{w}^{n+\eta} = \eta\mathbf{w}^{n+1} + (1-\eta)\mathbf{w}^{n} \\
&\mathbf{x}^{n+\eta} = \eta\mathbf{x}^{n+1} + (1-\eta)\mathbf{x}^{n} \\
&\dot{\mathbf{x}}^{n+\frac{1}{2}} \ = \ \frac{\mathbf{x}^{n+1} - \mathbf{x}^{n}}{\Delta t} \\
&\mathbf{M}\ddot{\mathbf{q}}^{n+1} + \mathbf{D}\dot{\mathbf{q}}^{n+1} + \mathbf{K}\mathbf{q}^{n+1} \ = \ \mathbf{f}^{ext}(\mathbf{w}^{n+1}(\mathbf{x}, t)) \\
&\widetilde{\mathbf{M}}\ddot{\mathbf{x}}^{n+1} + \widetilde{\mathbf{D}}\dot{\mathbf{x}}^{n+1} + \widetilde{\mathbf{K}}\mathbf{x}^{n+1} \ = \ \mathbf{K}_{c}\,\mathbf{q}^{n+1}
\end{aligned}
\tag{33}
$$

In many aeroelastic problems such as flutter analysis, a steady flow is first computed around a structure in equilibrium. Next, the structure is perturbed via an initial displacement and/or velocity and the aeroelastic response of the coupled fluid/structure system is analyzed. This suggests that a natural sequencing for the staggered time-integration of Eqs. (33) is:

1. Perturb the structure via some initial conditions.

2. Update the fluid grid to conform to the new structural boundary.

3. Advance the flow with the new boundary conditions.

4. Advance the structure with the new pressure load.

5. Repeat from step (2) until the goal of the simulation (flutter detection or suppression) is reached.

An important feature of partitioned solution procedures is that they allow the use of existing single discipline software modules. In this effort, we are particularly interested in re-using a 3D version of the massively parallel explicit flow solver described by Farhat, Lanteri and Fezoui [10,12,14,23].

Therefore, we select to time-integrate the semi-discrete fluid equations with a 3-step variant of the explicit Runge-Kutta algorithm. On the other hand, the aeroelastic response of a structure is often dominated by low frequency dynamics. Hence, the structural equations are most efficiently solved by an implicit time-integration scheme. Here, we select to time-integrate the structural motion with the implicit midpoint rule (IMR) because it allows enforcing both continuity Eqs. (2) while still

respecting the GCL condition (see [24]). Consequently, we propose the following explicit/implicit solution algorithm for solving the three-field coupled problem (33):

1. Update the fluid grid:

$$\begin{aligned} &\textit{Solve} \quad \widetilde{\mathbf{M}}\ddot{\mathbf{x}}^{n+1} + \widetilde{\mathbf{D}}\dot{\mathbf{x}}^{n+1} + \widetilde{\mathbf{K}}\mathbf{x}^{n+1} = \mathbf{K}_c\,\mathbf{q}^n \\ &\textit{Compute} \quad \mathbf{x}^{m1},\ \mathbf{x}^{m2} \quad \text{from Eq. (33)} \\ &\dot{\mathbf{x}}^{n+\frac{1}{2}} = \frac{\mathbf{x}^{n+1} - \mathbf{x}^n}{\Delta t} \end{aligned}$$

2. Advance the fluid system using RK3:

$$\begin{aligned} W_i^{n+1^{(0)}} &= W_i^n \\ W_i^{n+1^{(k)}} &= \frac{V_i(\mathbf{x}^n)}{V_i(\mathbf{x}^{n+1})} W_i^{n+1^{(0)}} \\ &+ \frac{1}{V_i(\mathbf{x}^{n+1})} \frac{1}{4-k} \frac{\Delta t}{2} (F_i(\mathbf{w}^n,\ \mathbf{x}^{m1},\ \dot{\mathbf{x}}^{n+\frac{1}{2}}) \\ &+ F_i(\mathbf{w}^n,\ \mathbf{x}^{m2},\ \dot{\mathbf{x}}^{n+\frac{1}{2}})) \quad k = 1,\ 2,\ 3 \\ W_i^{n+1} &= W_i^{n+1^{(3)}} \end{aligned} \tag{34}$$

3. Advance the structural system using IMR:

$$\begin{aligned} \mathbf{M}\ddot{\mathbf{q}}^{n+1} + \mathbf{D}\dot{\mathbf{q}}^{n+1} + \mathbf{K}\mathbf{q}^{n+1} &= \mathbf{f}^{ext}(\mathbf{w}^{n+1}) \\ \mathbf{q}^{n+1} &= \mathbf{q}^n + \frac{\Delta t}{2}(\dot{\mathbf{q}}^n + \dot{\mathbf{q}}^{n+1}) \\ \dot{\mathbf{q}}^{n+1} &= \dot{\mathbf{q}}^n + \frac{\Delta t}{2}(\ddot{\mathbf{q}}^n + \ddot{\mathbf{q}}^{n+1}) \end{aligned}$$

In the sequel the above explicit/implicit staggered procedure is referred to as A0. It is graphically depicted in Figure I.3. Extensive experiments with this solution procedure have shown that its stability limit is governed by the critical time-step of the explicit fluid solver (and therefore is not worse than that of the underlying fluid explicit time-integrator).

The 3-step Runge-Kutta algorithm is third-order accurate for linear problems and second-order accurate for nonlinear ones. The midpoint rule is second-order accurate. A simple Taylor expansion shows that the partitioned procedure A0 is first-order accurate when applied to the linearized Eqs. (32). When applied to Eqs. (33), its accuracy depends on the solution scheme selected for solving the fluid mesh equations of motion. As long as the time-integrator applied to these equations is

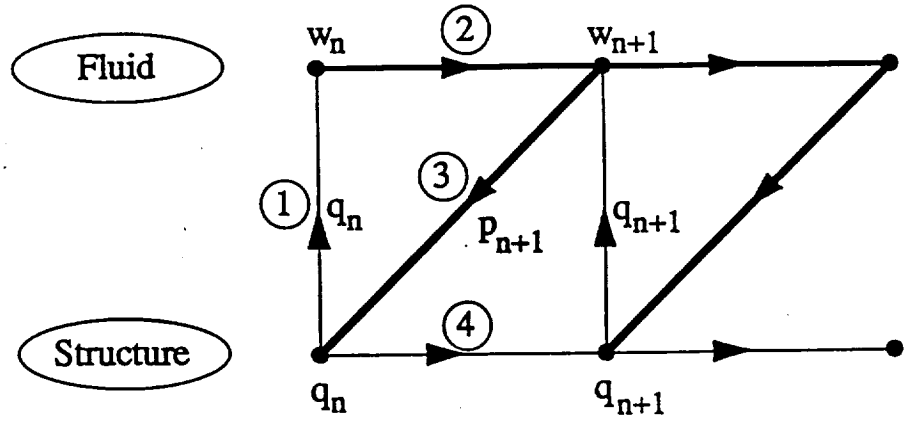

Figure I.3. The basic FSI staggered procedure A0.

consistent, A0 is guaranteed to be at least first-order accurate.

I.4. SUBCYCLING

The fluid and structure fields have often different physical time scales. For problems in aeroelasticity, the fluid flow usually requires a smaller temporal resolution than the structural vibration. Therefore, if A0 is used to solve Eqs. (33), the coupling time-step Δt_c will be typically dictated by the stability time-step of the fluid system Δt_F and not the time-step $\Delta t_S > \Delta t_F$ that meets the accuracy requirements of the structural field.

Subcycling the fluid computations with a factor $n_{S/F} = \Delta t_S / \Delta t_F$ can offer substantial computational advantages, including

- savings in the overall simulation CPU time, because in that case the structural field will be advanced fewer times.

- savings in I/O transfers and/or communication costs when computing on a heterogeneous platform, because in that case the fluid and structure kernels will exchange information fewer times.

However, these advantages are effectively realized only if subcycling does not restrict the stability region of the staggered algorithm to values of the coupling time-step Δt_c that are small enough to offset these advantages. In Ref. [31] it is shown that for the linearized problem (32), the straight forward conventional subcycling procedure — that is, the scheme where at the end of each $n_{S/F}$ fluid subcycles only the interface pressure computed during the last fluid subcycle is transmitted to the structure — lowers the stability limit of A0 to a value that is less than the critical time-step of the fluid explicit time-integrator.

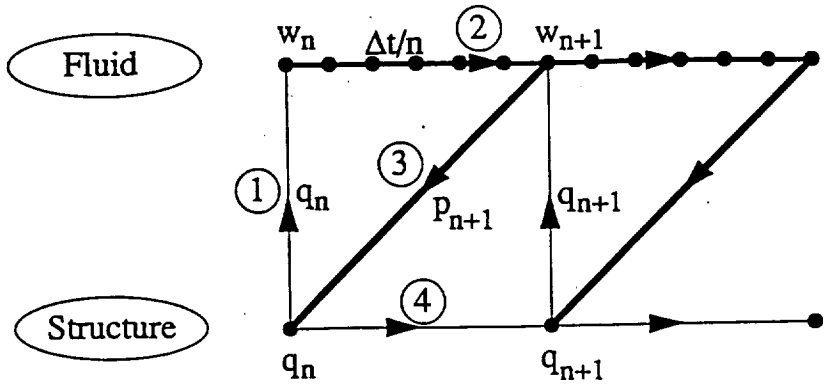

Figure I.4. The fluid-subcycled staggered algorithm A1.

On the other hand, it is also shown in Ref. [31] that when solving Eqs. (32), the stability limit of A0 can be preserved if: (a) the deformation of the fluid mesh between t^n and t^{n+1} is evenly distributed among the $n_{S/F}$ subcycles, and (b) at the end of each $n_{S/F}$ fluid subcycles, the average of the interface pressure field $\overline{p}_{\Gamma_{F/S}}$ computed during the subcycles between t^n and t^{n+1} is transmitted to the structure. Hence, a generalization of A0 is the explicit/implicit fluid-subcycled partitioned procedure depicted in Figure I.4 for solving Eqs. (33). This algorithm is denoted by A1.

Extensive numerical experiments have shown that for small values of $n_{S/F}$, the stability limit of A1 is governed by the critical time-step of the explicit fluid solver. However, experience has also shown that there exists a maximum subcycling factor beyond which A1 becomes numerically unstable. From the theory developed in [12] for the linearized Eqs. (32), it follows that A1 is first-order accurate, and that as one would have expected, subcycling amplifies the fluid errors by the factor $n_{S/F}$.

I.5. EXPLOITING INTER-FIELD PARALLELISM

Both algorithms A0 and A1 are inherently sequential. In both of these procedures, the fluid system must be updated before the structural system can be advanced. Of course, A0 and A1 allow intra-field parallelism (parallel computations within each system), but they inhibit inter-field parallelism. Advancing the fluid and structural systems simultaneously is appealing because it can reduce the total simulation time.

A simple variant of A1 (or A0 if subcycling is not desired) that allows inter-field parallel processing is graphically shown in Figure I.5. This variant is called A2.

Using A2, the fluid and structure kernels can run in parallel during the time-interval $[t_n,\ t_{n+n_{S/F}}]$. Inter-field communication or I/O transfer is needed only at the beginning of each time-interval. The

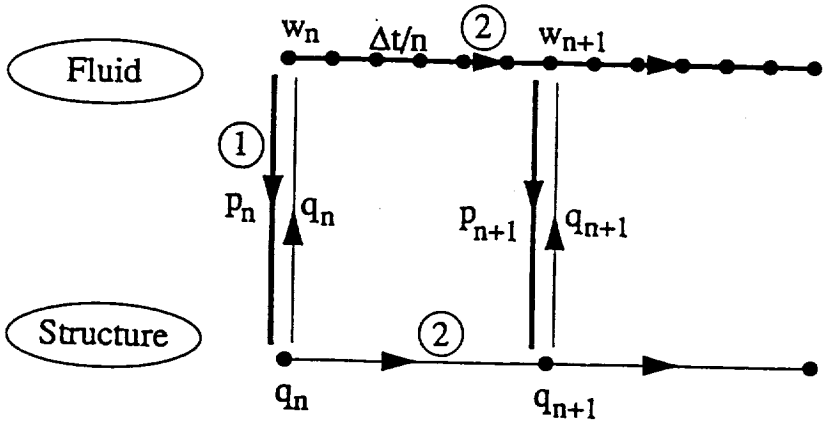

Figure I.5. The inter-parallel, fluid-subcycled staggered algorithm A2.

theory developed in Ref. [31] shows that for the linearized Eqs. (32), A2 is first-order accurate, but parallelism is achieved at the expense of amplified errors in the fluid and structure responses.

In order to improve the accuracy of the basic parallel time-integrator A2, we have investigated exchanging information between the fluid and structure kernels at half-steps as illustrated in Figure I.6. The resulting algorithm is called A3.

For algorithm A3, the first half of the computations is identical to that of A2, except that the fluid system is subcycled only up to $t^{n+\frac{n_{S/F}}{2}}$, while the structure is advanced in one step up to $t^{n+n_{S/F}}$. At the time $t^{n+\frac{n_{S/F}}{2}}$, the fluid and structure kernels exchange pressure, displacement and velocity information. In the second-half of the computations, the fluid system is subcycled from $t^{n+\frac{n_{S/F}}{2}}$ to $t^{n+n_{S/F}}$ using the new structural information, and the structural behavior is re-computed in parallel using the newly received pressure distribution. Note that the first evaluation of the structural state vector can be interpreted as a predictor.

It can be shown that when applied to the linearized Eqs. (32), A3 is first-order accurate and reduces the errors of A2 by the factor $n_{S/F}$, at the expense of one additional communication step or I/O transfer during each coupled cycle (see [12] for a detailed error analysis).

I.6. COMPUTER IMPLEMENTATION ISSUES

I.6.1. Incompatible mesh interfaces

In general, the fluid and structure meshes have two independent representations of the physical fluid/structure interface. When these representations are identical — for example, when every fluid grid point on $\Gamma_{F/S}$ is also a structural node and *vice-versa* — the evaluation of the pressure forces and the transfer of the structural motion to the fluid mesh are trivial operations. However, analysts

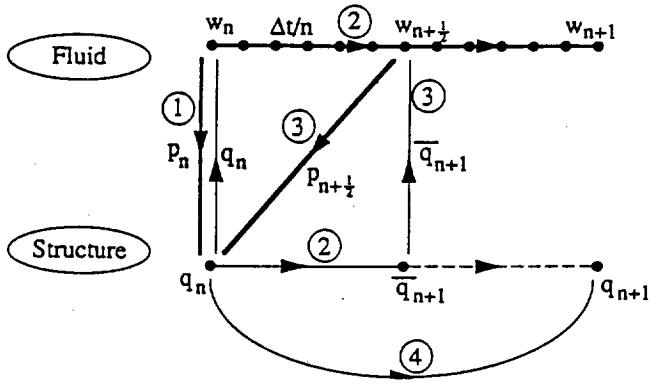

Figure I.5. The midpoint-corrected, inter-parallel, fluid-subcycled staggered algorithm A3.

usually prefer to be free of such restrictions. In particular:

- Be able to use a fluid mesh and a structural model that have been independently designed and validated.
- Be able to refine each mesh independently from the other.

Hence, most realistic aeroelastic simulations will involve handling fluid and structural meshes that are incompatible at their interface boundaries (Figure I.7). In Ref. [27], we have addressed this issue and proposed a preprocessing "matching" procedure that does not introduce any other approximation than those intrinsic to the fluid and structure solution methods. This procedure can be summarized as follows.

The nodal forces induced by the fluid pressure on the "wet" surface of a structural element e can be written as:

$$f_i = -\int_{\overline{\Omega}^{(e)}} N_i p \nu \, d\sigma \tag{35}$$

where $\overline{\Omega}^{(e)}$ denotes the geometrical support of the wet surface of the structural element e, p is the pressure field, ν is the unit normal to $\overline{\Omega}^{(e)}$, and N_i is the shape function associated with node i. Most if not all FE structural codes evaluate the integral in Eq. (35) via a quadrature rule:

$$f_i = -\sum_{g=1}^{g=n_g} w_g N_i(X_g) p(X_g) \tag{36}$$

where w_g is the weight of the Gauss point X_g. Hence, a structural code needs to know the values of the pressure field only at the Gauss points of its wet surface. This information can be easily

made available once every Gauss point of a wet structural element is paired with a fluid cell (Figure I.8). It should be noted that in Eq. (36), X_g are not necessarily the same Gauss points as those used for stiffness evaluation. For example, if a high pressure gradient is anticipated over a certain wet area of the structure, a larger number of Gauss points can be used for the evaluation of the pressure forces f_i on that area.

On the other hand, when the structure moves and/or deforms, the motion of the fluid grid points on $\Gamma_{F/S}$ can be prescribed via the regular FE interpolation:

$$\mathbf{x}(S_j) = \sum_{k=1}^{k=wne} N_k(\mathcal{X}_j)\mathbf{q}_k^{(e)} \tag{37}$$

where S_j, wne, $\mathcal{X}_j$, and $\mathbf{q}_k$ denote respectively a fluid grid point on $\Gamma_{F/S}$, the number of wet nodes in its "nearest" structural element e, the natural coordinates of S_j in $\overline{\Omega}^{(e)}$, and the structural displacement at the k-th node of element e. From Eq. (37), it follows that each fluid grid point on $\Gamma_{F/S}$ must be matched with one wet structural element (see Figure I.9).

Given a fluid grid and a structural model, constructed independently, the Matcher program described in Ref. [27] generates all the data structures needed to evaluate the quantities in Eqs. (39,40) in a single preprocessing step.

I.6.3. Intra-field parallel processing

Aeroelastic simulations are known to be computationally intensive and therefore can benefit from the parallel processing technology. An important feature of a partitioned solution procedure is preservation of software modularity. Hence, all of the solution procedures A0, A1, A2 and A3 can use existing computational fluid dynamics and computational structural mechanics parallel algorithms. The solution of the mesh motion equations can be easily incorporated into an existing fluid code, and its parallelization is not more difficult than that of a FE structural algorithm.

Our approach to parallel processing is based on the mesh partitioning/message-passing paradigm, which leads to a portable software design. Using an automatic mesh partitioning algorithm [13,17] both fluid and structural meshes are decomposed into subdomains. The same "old" serial code is executed within every subdomain. The "gluing" or assembly of the subdomain results is implemented in a separate software module.

This approach enforces data locality [23] and is therefore suitable for all parallel hardware architectures. Note that in this context, message-passing refers to the assembly phase of the subdomain results. It does not imply that messages have to be explicitly exchanged between the subdomains. For example, message-passing can be implemented on a shared memory multiprocessor as a simple access to a shared buffer, or as a duplication of one buffer into another.

I.6.4. Inter-field parallel processing

Using the message-passing paradigm, inter-field parallel processing can be implemented in the same manner as intra-field multiprocessing. The fluid and structure codes can run either on different sequential or parallel machines, or on a different partition of the same multiprocessor. Any

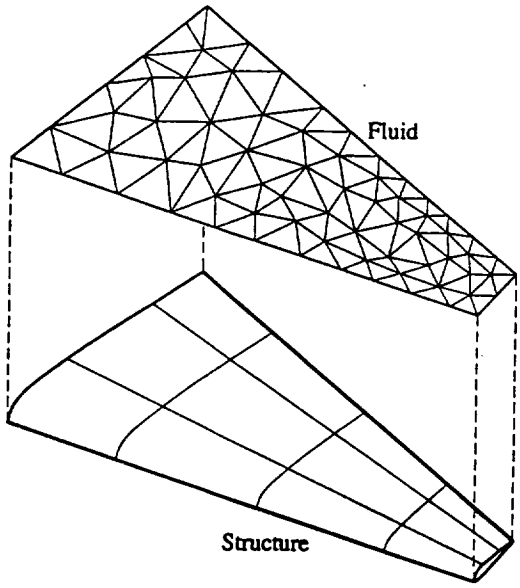

Figure I.7. Mismatched fluid-structure discrete interfaces.

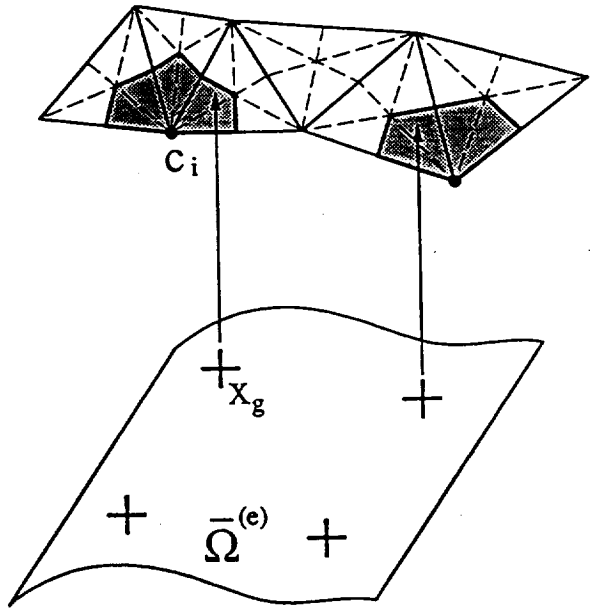

Figure I.8. Pairing of structural Gauss points and fluid cells.

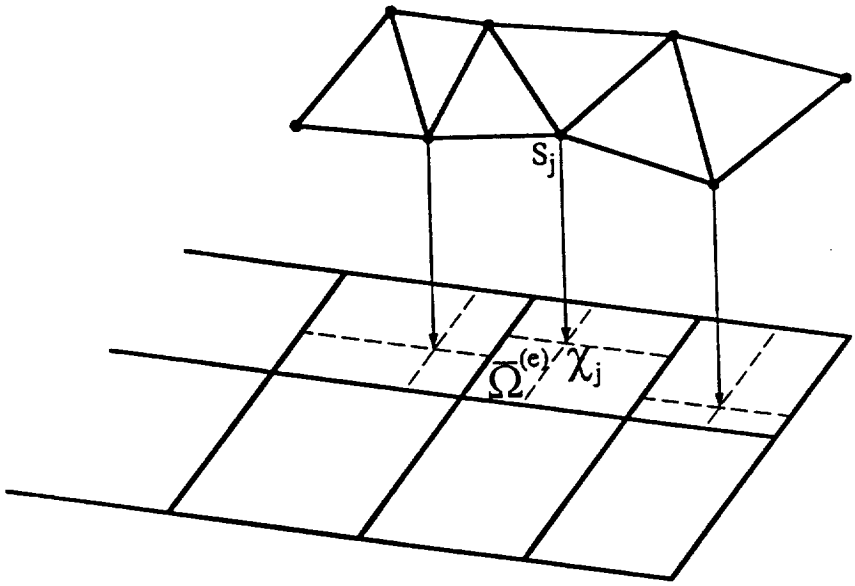

Figure I.9. Pairing of fluid point and wet structural element

software product such as PVM [19] can be used to implement message-passing between the two computational kernels.

I.7. APPLICATIONS AND PRELIMINARY RESULTS

I.7.1. Transonic Wing Benchmark (3D)

Here we illustrate the aeroelastic computational methodology described in the previous sections with some preliminary numerical investigations on an iPSC-860, a Paragon XP/S, a Cray T3D, and an IBM SP2 massively parallel systems, of the aerodynamics and aeroelastic transient response of a 3D wing in a transonic airstream.

The wing is represented by an equivalent plate model discretized by 1071 triangular plate elements, 582 nodes, and 6426 degrees of freedom (Figure I.10). Four meshes identified as M1 through M4, are designed for the discretization of the 3D flow domain around the wing. The characteristics of theses meshes are given in Table I.1 where N_{ver}, N_{tet}, N_{fac}, and N_{var} denote respectively the number of vertices, tetrahedra, facets (edges), and fluid variables, respectively. A partial view of the discretization of the flow domain is shown in Figure 11.

The sizes of the fluid meshes M1–M4 have been tailored for parallel computations on respectively 16 (M1), 32 (M2), 64 (M3), and 128 processors (M4) of a Paragon XP/S and a Cray T3D systems. In particular, the sizes of these meshes are such that the processors of a Paragon XP/S machine with 32 Mbytes per node would not swap when solving the corresponding flow problems.

Because the fluid and structural meshes are not compatible at their interface (Figure I.12), the Matcher software [27] is used to generate in a single preprocessing step the data structures required for transferring the pressure load to the structure, and the structural deformations to the fluid.

Table I.1 Characteristics of the fluid meshes M1–M4 for 3D benchmark

Mesh	N_{var}	N_{tet}	N_{fac}	N_{var}
M1	15460	80424	99891	77300
M2	31513	161830	201479	157565
M3	63917	337604	415266	319585
M4	115351	643392	774774	576755

I.7.1. The Flow Solver and its Parallelization

The Euler flow equations are solved with a second-order accurate FV Monotonic Upwinding Scheme for Conservation Laws (MUSCL) [41,28] on fully unstructured grids. The resulting semi-discrete equations are time-integrated using a second-order low-storage explicit Runge-Kutta method. Further details regarding this explicit unstructured flow solver and its subdomain based parallelization can be found in recent publications [10,12,14,23].

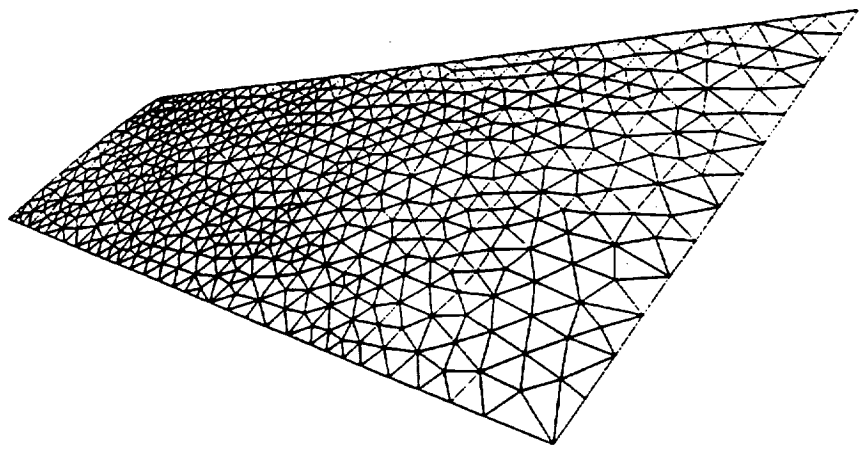

Figure I.10. The discrete structural model.

I.7.2. The Mesh Motion Solver

In this work, the unstructured dynamic fluid mesh is represented by the pseudo-structural model of Batina [3] ($\widetilde{\mathbf{M}} = \widetilde{\mathbf{D}} = 0$). The grid points located on the upstream and downstream boundaries are held fixed. The motion of those points located on $\Gamma_{F/S}$ is determined from the wing surface

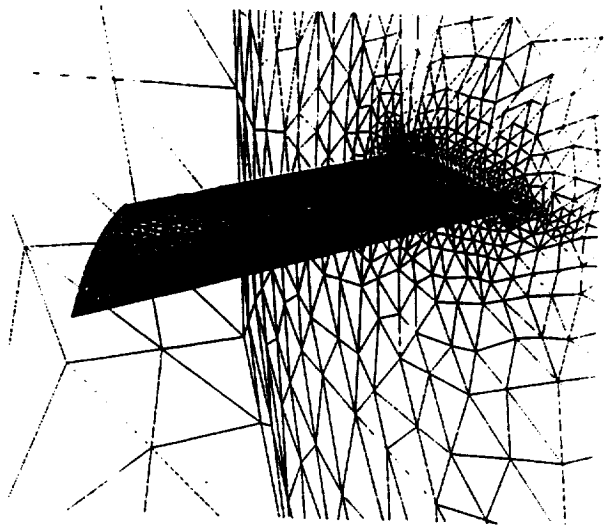

Figure I.11. The discrete flow domain (partial view).

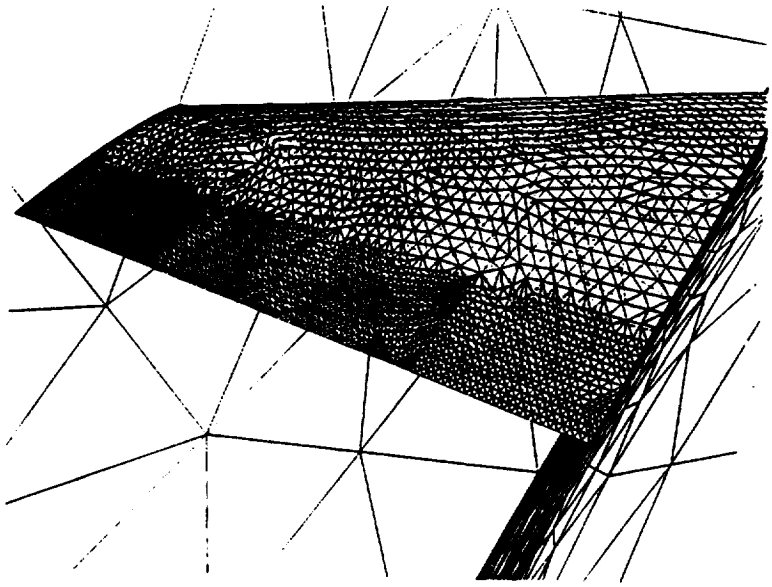

Figure I.12. Fluid/structure interface incompatibilities

motion and/or deformation. At each time-step t^{n+1}, the new position of the interior grid points is determined from the solution of the displacement driven pseudo-structural problem via the two-step iterative procedure described in [14].

I.7.3. The Parallel Structure Solver

The structural equations of dynamic equilibrium are solved with the parallel implicit transient Finite Element Tearing and Interconnecting (FETI) method [15]. Because it is based on a midpoint rule formulation, this method allows enforcing both continuity Eqs. (2) while still respecting the GCL

condition. The resistance of the structure to displacements in the plane of the skin is assumed to be small. Consequently, all structural computations are performed with a linearized structural theory. Since the FETI solver is a domain decomposition based iterative solver, we also use the special restarting procedure proposed in Ref. [16] for the efficient iterative solution of linear systems with repeated right hand sides.

I.7.4. Computational Platforms

Computations were performed on the following massively parallel computers: Intel iPSC-860 hypercube, Intel Paragon XP/S, Cray T3D, and IBM SP2, using double precision floating-point arithmetic throughout. Message passing is carried out via NX on the Paragon XP/S multiprocessor, PVM T3D on the Cray T3D system, and MPI on the IBM SP2. On the hypercube, fluid and structure solvers are implemented as separate programs that communicate via the intercube communication procedures described by Barszcz [2].

I.7.5. Performance of the Parallel Flow Solver

The performance of the parallel flow solver is assessed with the computation of the steady state of a flow around the given wing at a Mach number $M_\infty = 0.84$ and an angle of attack $\beta = 3.06$ degrees. The CFL number is set to 0.9. The four meshes M1–M4 are decomposed in respectively 16, 32, 64, and 128 *overlapping* subdomains using the mesh partitioner described in [26]. The motivation for employing overlapping subdomains and the impact of this computational strategy on parallel performance are discussed in Ref. [14]. Measured times in seconds are reported in Tables I.2 through I.4 for the first 100 time steps on a Paragon XP/S machine (128 processors), a Cray T3D system (128 processors), and an IBM SP2 computer (128 processors), respectively. In these tables, N_p, N_{var}, T^{loc}_{comm}, T^{glo}_{comm}, T_{comp}, T_{tot} and Mflops denote respectively the number of processors, the number of variables (unknowns) to be solved, the time elapsed in short range interprocessor communication between neighboring subdomains, the time elapsed in long range global interprocessor communication, the computational time, the total simulation time, and the computational speed in millions of floating point operations per second. Communication and computational times were not measured separately on the SP2.

Typically, short range communication is needed for assembling various subdomain results such as fluxes at the subdomain interfaces, and long range interprocessor communication is required for reduction operations such as those occurring in the the evaluation of the stability time-steps and the norms of the nonlinear residuals. It should be noted that we use the same fluid code for steady state and aeroelastic computations. Hence, even though we are benchmarking in Tables 2-4 a steady state computation with a local time stepping strategy, we are still timing the kernel that evaluates the global time-step in order to reflect its impact on the unsteady computations that we perform in aeroelastic simulations such as those that are discussed next. The megaflop rates reported in Tables I.2 through I.4 are computed in a conservative manner: they exclude all the redundant computations associated with the overlapping subdomain regions.

It may be readily verified that the number of processors assigned to each mesh is such that N_{var}/N_p is almost constant. This means that larger numbers of processors are attributed to larger meshes

Table I.2. Performance of the parallel flow solver on the Paragon XP/S system for 16–128 processors (100 time steps — CFL = 0.9)

Mesh	N_p	N_{var}	T_{comm}^{loc}	T_{comm}^{glo}	T_{comp}	T_{tot}	Mflops
M1	16	77,300	2.0 s.	40.0 s.	96.0 s.	138.0 s.	84
M2	32	157,565	4.5 s.	57.0 s.	98.5 s.	160.0 s.	145
M3	64	319,585	7.0 s.	90.0 s.	103.0 s.	200.0 s.	240
M4	128	576,755	6.0 s.	105.0 s.	114.0 s.	225.0 s.	401

Table I.3. Performance of the parallel flow solver on the Cray T3D system for 16–128 processors (100 time steps — CFL = 0.9)

Mesh	N_p	N_{var}	T_{comm}^{loc}	T_{comm}^{glo}	T_{comp}	T_{tot}	Mflops
M1	16	77,300	1.6 s.	2.1 s.	87.3 s.	91.0 s.	127
M2	32	157,565	2.5 s.	4.1 s.	101.4 s.	108.0 s.	215
M3	64	319,585	3.5 s.	7.2 s.	100.3 s.	111.0 s.	433
M4	128	576,755	3.0 s.	7.2 s.	85.3 s.	95.5 s.	945

Table I.4. Performance of the parallel flow solver on the IBM SP2 system for 16–128 processors (100 time steps — CFL = 0.9)

Mesh	N_p	N_{var}	T_{comm}^{loc}	T_{comm}^{glo}	T_{comp}	T_{tot}	Mflops
M1	16	77,300				10.8 s.	1072
M2	32	157,565				12.0 s.	1930
M3	64	319,585				12.8 s.	3785
M4	128	576,755				11.9 s.	7430

in order to keep each local problem within a processor at an almost constant size. For such a benchmarking strategy, *parallel scalability* of the flow solver on a target parallel processor implies that the total solution CPU time should be constant for all meshes and their corresponding number of processors.

This is clearly not the case for the Paragon XP/S system. On this machine, short range communica-

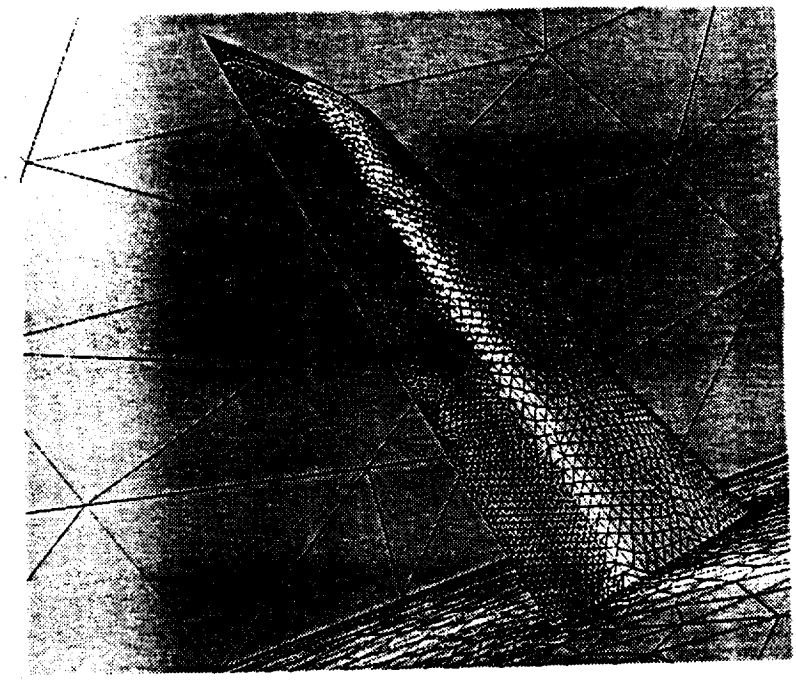

Figure I.13. Mach number isosurfaces for the steady-state regime.

tion is shown to be inexpensive, but long range communication costs are observed to be important. This is due to the latency of the Paragon XP/S parallel processor, which is an order of magnitude slower than that of the Cray T3D system. Another possible source of global communication time increase is the load imbalance between the processors since message passing is also used for synchronization. However, this does not seem to be significant on the T3D and SP2 parallel processors.

On the other hand, parallel scalability is well demonstrated for the Cray T3D and IBM SP2 systems. The results reported in Tables I.3 and I.4 show that all computations using meshes M1–M4 and the corresponding number of processors consume almost the same total amount of CPU time. For 128 processors, the Cray T3D system is shown to be more than twice faster than the Paragon XP/S machine. The difference appears to be strictly in long range communication as the computational time is reported to be almost the same on both machines. However, most impressive is the fact that an IBM SP2 with 32 processors only is shown to be three times faster than a 128-processor Paragon XP/S, and faster than a Cray T3D with 128 processors.

I.7.6. Performance of the Parallel Structure Solver

For the performance assessment of the parallel FETI structural solver, we refer the reader to the recent publications [15,16].

I.7.7. Performance of the Partitioned Procedures A0–A3

In order to illustrate the relative merits of the partitioned procedures A0, A1, A2 and A3, we consider first two different series of transient aeroelastic simulations at Mach number $M_\infty = 0.84$ that highlight

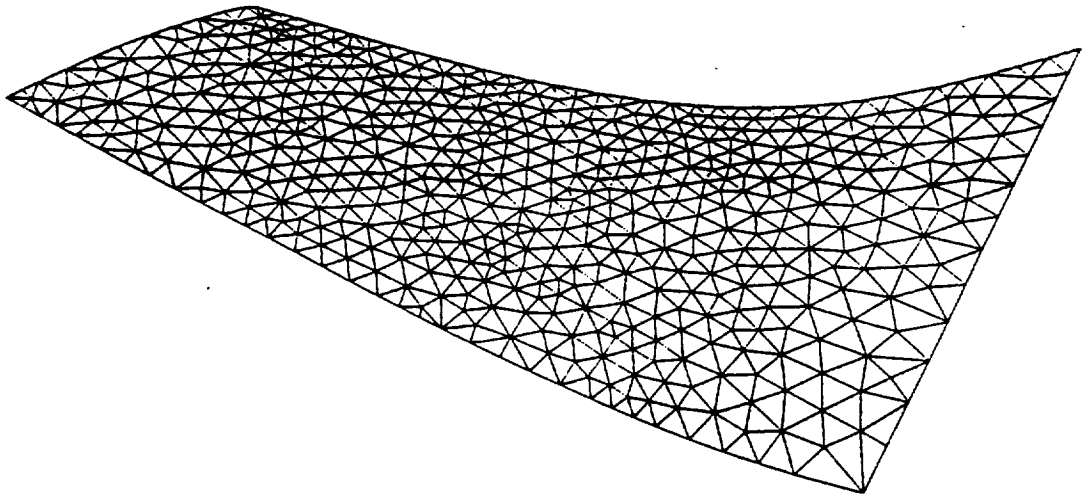

Figure I.14. Initial perturbation of the displacement field of the wing.

- the relative accuracy of these coupled solution algorithms for a fixed subcycling factor $n_{S/F}$.
- the relative speed of these coupled solution algorithms for a fixed level of accuracy.

In all cases, mesh $M2$ is used for the flow computations, 32 processors of an iPSC-860 system are allocated to the fluid solver, and 4 processors of the same machine are assigned to the structural code. Initially, a steady-state flow is computed around the wing at $M_\infty = 0.84$ (Figure I.13), a Mach number at which the wing described above is not supposed to flutter. Then, the aeroelastic response of the coupled system is triggered by a displacement perturbation of the wing along its first mode (Figure I.14).

First, the subcycling factor is fixed to $n_{S/F} = 10$ then to $n_{S/F} = 30$, and the lift is computed using a time-step corresponding to the stability limit of the explicit flow solver in the absence of coupling with the structure. The obtained results are depicted in Figure I.15 and Figure I.16 for the first half cycle.

The superiority of the parallel fluid-subcycled A3 solution procedure is clearly demonstrated in Figure I.15 and Figure I.16. For $n_{S/F} = 10$, A3 is shown to be the closest to A0, which is supposed to be the most accurate since it is sequential and non-subcycled. A1 and A2 have comparable accuracies. However, both of these algorithms exhibit a significantly more important phase error than A3, especially for $n_{S/F} = 30$.

Next, the relative speed of the partitioned solution procedures is assessed by comparing their CPU time for a certain level of accuracy dictated by A0. For this problem, it turned out that in order to meet the accuracy requirements of A0, the solution algorithms A1 and A2 can subcycle only up to

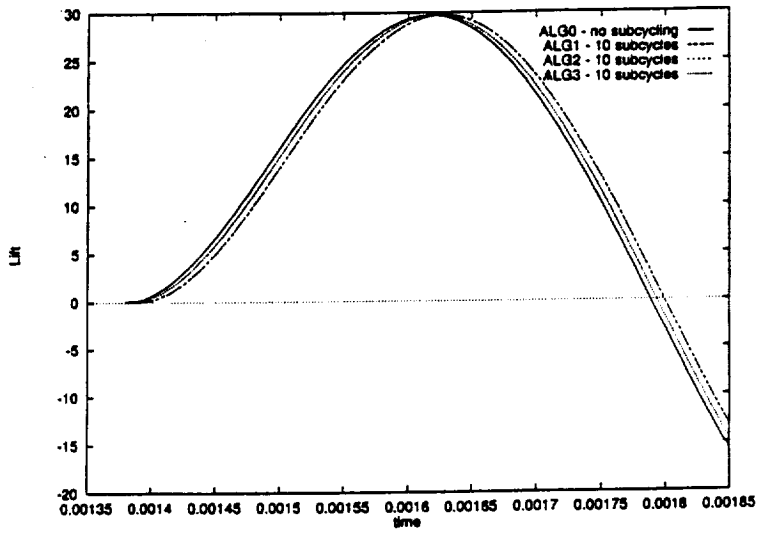

Figure I.15. Lift history for the first half cycle, $n_{S/F} = 10$

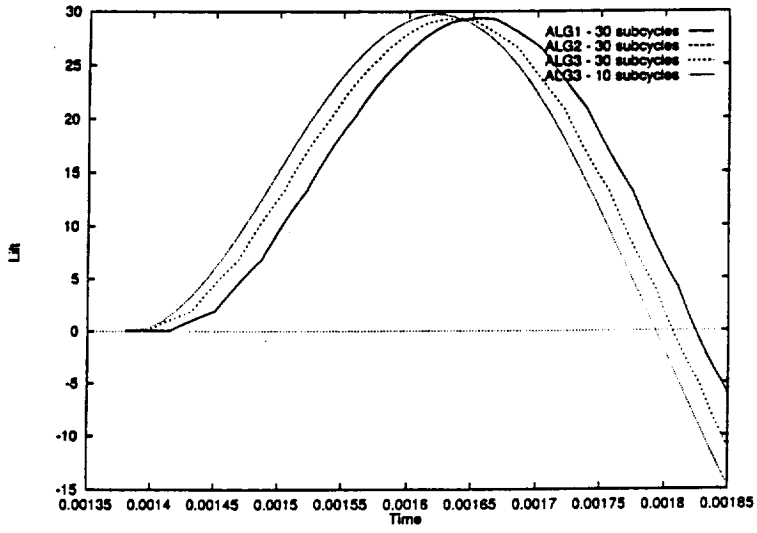

Figure I.16. Lift history for the first half cycle, $n_{S/F} = 30$

$n_{S/F} = 5$, while A3 can easily use a subcycling factor as large as $n_{S/F} = 10$. The performance results measured on an iPSC-860 system are reported on Table I.5 for the first 50 coupled time-steps. In this table, ICWF and ICWS denote the inter-code communication timings measured respectively in the fluid and structural kernels; these timings include idle and synchronization (wait) time when the fluid and structural communications do not completely overlap. For programming reasons, ICWS is monitored together with the evaluation of the pressure load.

Table I.5. Performance results for coupled FSI problem on the Intel iPSC-860
Fluid: 32 processors, Structure: 4 processors
Elapsed time for 50 fluid time-steps

Alg.	Fluid Solver	Fluid Motion	Struc. Solver	ICWS	ICWF	Total CPU
A0	177.4 s.	71.2 s.	33.4 s.	219.0 s.	384.1 s.	632.7 s.
A1	180.0 s.	71.2 s.	16.9 s.	216.9 s.	89.3 s.	340.5 s.
A2	184.8 s.	71.2 s.	16.6 s.	114.0 s.	0.4 s.	256.4 s.
A3	176.1 s.	71.2 s.	10.4 s.	112.3 s.	0.4 s.	247.7 s.

I.8. CONCLUSIONS

From the results reported in Table I.5, the following observations can be made.

- The fluid computations dominate the simulation time. This is partly because the structural model is simple in this case, and a linear elastic behavior is assumed. However, by allocating 32 processors to the fluid kernel and 4 processors to the structure code, a reasonable load balance is shown to be achieved for A0.

- During the first 50 fluid time-steps, the CPU time corresponding to the structural solver does not decrease linearly with the subcycling factor $n_{S/F}$ because of the initial costs of the FETI reorthogonalization procedure designed for the efficient iterative solution of implicit systems with repeated right hand sides [16].

- The effect of subcycling on intercube communication costs is clearly demonstrated. The impact of this effect on the total CPU time is less important for A2 and A3 which feature inter-field parallelism in addition to intra-field multiprocessing, than for A1 which features intra-field parallelism only (note that A1 with $n_{S/F} = 1$ is identical to A0), because the flow solution time is dominating.

- Algorithms A2 and A3 allow a certain amount of overlap between inter-field communications, which reduces intercube communication and idle time on the fluid side to less than 0.001% of the amount corresponding to A0.

- The superiority of A3 over A2 is not clearly demonstrated for this problem because of the simplicity of the structural model and the consequent load unbalance between the fluid and structure computations.

Most importantly, the performance results reported in Table 5 demonstrate that subcycling and inter-field parallelism are desirable for aeroelastic simulations even when the flow computations dominate the structural ones, because these features can significantly reduce the total simulation time by minimizing the amount of inter-field communications and overlapping them. For the simple problem described herein, the parallel fluid-subcycled A2 and A3 algorithms are more than twice faster than the conventional staggered procedure A0.

Acknowledgments

This work was supported by NASA Langley under Grant NAG-1536427, by NASA Lewis Research Center under Grant NAG3-1273, and by the National Science Foundation under Grant ASC-9217394.

Appendix II

LB: A Program for Load-Balancing Multiblock Grids

Summary

This Appendix describes recent research towards load-balancing the execution of ENG10 on parallel machines. ENG10 is a multiblock-multigrid code developed by Mark Stewart of NYMA Research Inc. to perform axisymmetric aerodynamic analysis of complete turbofan engines taking into account combustion, compression and mixing effects through appropriate circumferential averaging. The load-balancing process is based on an iterative strategy for subdividing and recombining the original grid-blocks that discretize distinct portions of the computational domain. The research work reported here was performed by U. Gumaste under the supervision of Prof. C. A. Felippa.

II.1. INTRODUCTION

II.1.1. Motivation

For efficient parallelization of multiblock-grid codes, the requirement of load balancing demands that the grid be subdivided into subdomains of similar computational requirements, which are assigned to individual processors. Load balancing is desirable in the sense that if the computational load of one or more blocks substantially dominates that of others, processors given the latter must wait until the former complete.

Such "computational bottlenecks" can negate the beneficial effect of parallelization. To give an admittedly extreme example, suppose that the aerodynamic discretization uses up 32 blocks which are assigned to 32 processors, and that one of them takes up 5 times longer to complete than the average of the remaining blocks. Then 31 processors on the average will be idle 80% of the time.

Load balancing is not difficult to achieve for unstructured meshes arising with finite-element or finite-volume discretizations. This is because in such cases one deals with element-level granularity, which can be efficiently treated with well studied domain-decomposition techniques for unstructured meshes. In essence such subdomains are formed by groups of connected elements, and elements may be moved from one domain to another with few "strings attached" other than connectivity.

On the other hand for multiblock-grid discretizations the problem is more difficult and has not, to the writers' knowledge, been investigated in any degree of generality within the context of load balancing. The main difficulty is that blocks cannot be arbitrarily partitioned, for example cell by cell, because discretization constraints enforcing grid topological regularity must be respected.

The following is an outline of the program LB developed at the University of Colorado to perform load-balancing of the multiblock discretization used in the program ENG10. This is a multiblock-multigrid code developed by Mark Stewart of NYMA Research Inc. to perform axisymmetric

aerodynamic analysis of complete turbofan engines taking into account combustion, compression and mixing effects through appropriate circumferential averaging [35].

II.1.2. Requirements and Constraints

Multiblock grids are used to discretize complex geometries. A multiblock grid divides the physical subdomain into topologically rectangular blocks. The grid pertaining to each block is regular (structured). For bladed jet engine geometries, this is achieved by a series of programs also written by Mark Stewart, namely TOPOS, TF and MS [36,37], which function as preprocessors to ENG10.

Efficient parallelization requires the computational load to be (nearly) equal among all processors. Usually, depending upon the geometry, the computational sizes of component blocks of a multiblock discretization vary and mapping one to each processor would not naturally ensure load balance. The LB program attempts to load balance a given multiblock grid so that the resulting subdivisions of the grid are of similar computational cost.

For re-use of ENG10 to be possible for the parallel version, it is required that the resulting subdivisions of the original multiblock grid be also regular grids or are collections of blocks, each of which contain regular grids. This imposed the restriction that the number of final subdivisions desired be greater than the number of blocks in the original grid. Thus for most cases, ideally, the number of blocks in the original grid should be 10 to 20, because 32 to 128 processors are normally used in present generation MPPs. LB works better when the number of available processor substantially exceeds the original number of blocks.

II.1.3. Multiblock Grid and MS

MS is a program that, given the domain discretization and blade forces, loss and combustor heating data, etc., interpolates the data onto the grid. This program was used as a basis for LB as it possesses the data structures most amenable to the task of load balancing.

Blocks are arranged in a C programming language linked list. Each block possesses a set of segments that are lines joining grid points. The number of segments in each direction (transverse and lateral) determines the computational size of the block. Segments can be of different types depending upon where they are located as follows :

1. *False boundary segments.* These are segments located at the interface between blocks. These are called "false" boundaries as they are not actual physical boundaries in the grid but merely lines across which data has to be exchanged between two adjacent blocks. Knowledge about the false boundaries is essential to determine block connectivity.
2. *Internal and solid boundary segments.* These are segments located at the interface of combustors, blades, etc. Knowledge about the internal and solid boundary segments helps determine the location of blades, combustors and other engine components.
3. *Far-field boundary segments.* These are segments located at the far-field boundaries of the domain and are useful in imposing boundary conditions.

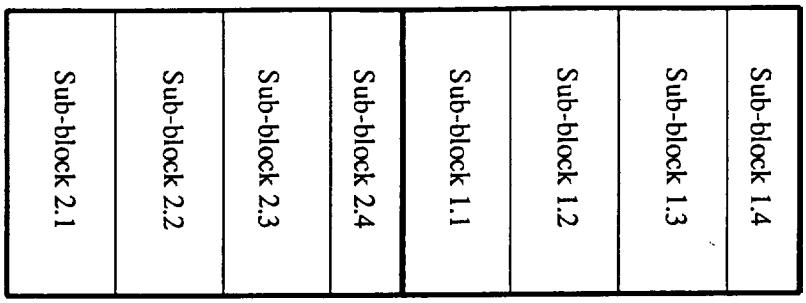

Figure II.1. Block division prior to merger.

II.2. ALGORITHM

A very simple yet efficient algorithm based purely on the geometry of the multiblock grid and block connectivity was adopted for this program.

The input file containing the grid gives information only about the coordinates of the grid points, block dimensions component segments and boundary data. Hence the first task is to determine the block connectivity. This is done by analysing the false boundary information and determining blocks across opposite sides of the same false boundary segment. Once the interconnectivity between blocks is established, the total number of cells in the grid is calculated and that divided by the number of final subdivisions desired gives an estimate of the *average* number of cells per subdivision.

Based on this average value, blocks are classified into "small" blocks and "large" blocks. Large blocks are those whose size is greater than the average size determined above, whereas small blocks have a size less than or equal to the average size.

Large blocks are then split into smaller blocks, each of which has a size approximately equal to the average size. Smaller blocks are collected into groups so that the total size of each group is equal to the average size. This has been found to give excellent load balance for small grids, grids in which block sizes are compatible, and grids for unbladed configurations. For more complex grids satisfactory results have been obtained.

II.3 IMPLEMENTATION

II.3.1 Maximum Block Merger

As first step, blocks from the original grid are merged as much as possible to generated larger blocks. This is done so as to maximize processor usage.

Consider two blocks as illustrated in Figure II.1. Assume that load-balancing conditions require

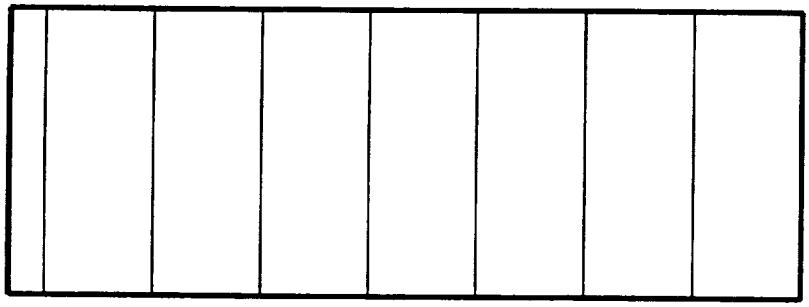

Figure II.2. Block after merger.

that each of the blocks be split into four blocks, vertically. Vertical splitting of blocks proceeds from right to left since blocks are stored in that manner. It is seen that sub-blocks 1.4 and 2.4 are clearly much smaller than the other sub-blocks and assigning an individual processor to each of them would be wasteful. Also, if the number of sub-blocks of each of the blocks is reduced to three from four, each of the processors will become overloaded. Therefore, the best solution to this problem is to first merge both the blocks and then split their combination to get a better load balance as shown in Figure II.2.

In this case it is seen that not only is the total number of sub-blocks reduced by one (implying that one less processor will be required) but also the load balancing is more effective since sub-block sizes are more compatible.

Blocks cannot be merged arbitrarily but only in those cases when the resulting larger block will have a regular grid. This is illustrated in Figure II.3. As can be seen in that figure, it is possible to merge block 1 with block 2 as their merging will result in the formation of a larger block in which the grid is regular. However, block 3 cannot be merged with either of block 1 or 2 as the resulting block would not have a top[ologically regular structure.

II.3.2. Block Classification

Once blocks are merged to the maximum permissible extent, all of them are passed through a classifying routine by which they are tagged as "small" or "large."

II.3.3. Splitting of "Large" Blocks

Those blocks classified as "large" blocks are split into smaller sub-blocks, each having a size as close as possible to the desired average size.

Blocks are split horizontally or vertically depending upon their dimensions. Wider blocks are split vertically and narrower blocks are split horizontally. Splitting of a block involves generation of a false boundary across the sub-blocks and checking for the presence of blades and other engine

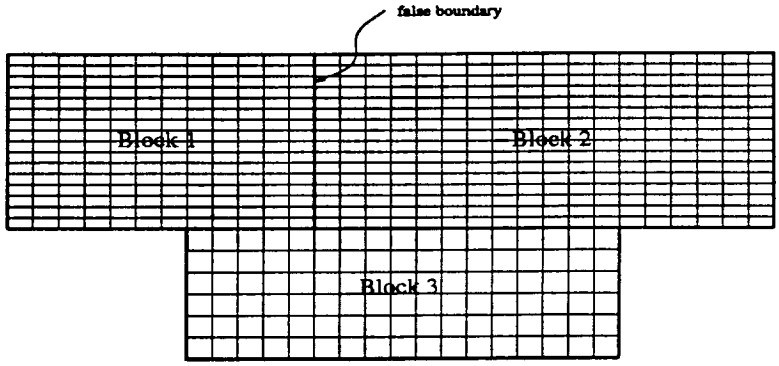

Figure II.3. Possible block mergers.

components which cannot be "cut". This is done to ensure continuity in these critical regions.

II.3.4 Re-merging and Grouping

Once all the "large" blocks are split, the second phase of the program begins in which the blocks are re-merged or grouped for maximum processor efficiency. This is done mainly to take very small blocks into consideration, which can be explained with the help of the Figure II.4.

In this situation, there is a cluster of "small" blocks with no "large" block nearby. The program selects a number of such "small" blocks and groups them into a cluster. Grouping is different from merging. Blocks are not merged to produce a single larger block but they are only meant to reside on the same processor. Grouping requires knowing block interconnectivity and proceeds in a recursive fashion. First, all "small" blocks adjacent to the present block are considered. Then, if the total number of cells of all the blocks is less than the average size, blocks adjacent to the block's adjacent blocks are examined. This goes on until a sufficient number of cells are obtained.

There is another case which arises after a "large" block has been split resulting in the generation of smaller sub-blocks, each being approximately equal to the average in size. In this case, again, the adjacent "small" blocks are merged into one of the children of the parent "large" block. Here, only one such block grouping is permitted since it should be noted that the "child" blocks are very close to the desired average size and the processor on which they reside should not be further loaded. This case is illustrated in Figure II.5.

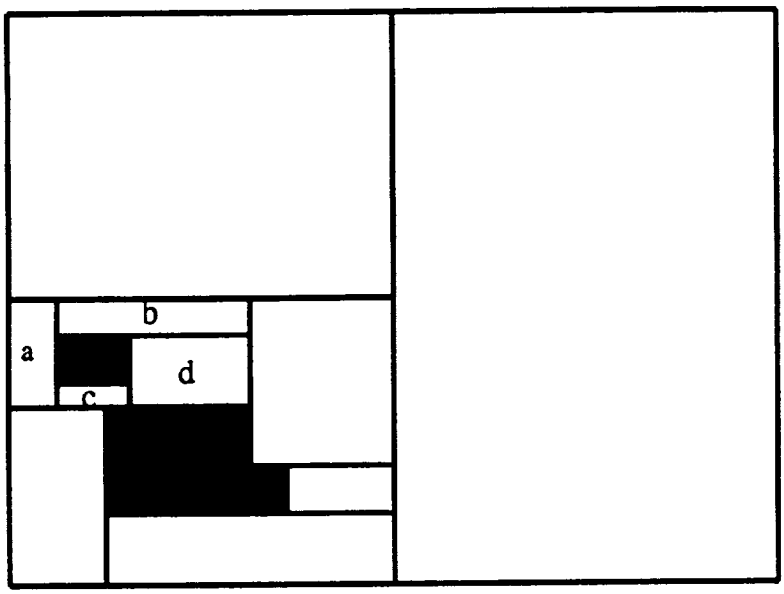

Blocks a, b, c and d would be "clustered"

Figure II.4. Grouping of small blocks.

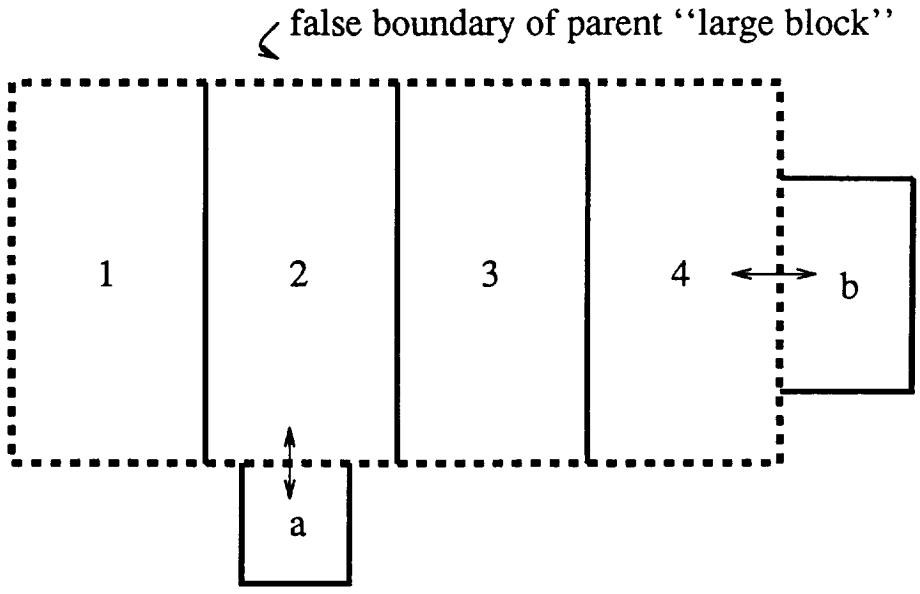

Figure II.5. Grouping of small and large blocks.

II.3.5 Some Practical Considerations

It has been observed after going through several test cases that the process of load-balancing for complex multiblock grids is not always deterministic and hence user inputs may be required to make the process more predictable. This input comprises the following parameters.

MAX_TOL This is the maximum tolerable value to which a processor can be loaded, expressed in terms of the average size. Usually values between 0.95 and 1.2 give sufficiently good results.

MIN_TOL This is the minimum tolerable value to which a processor can be loaded, expressed in terms of the average size. Usually values between 0.6 and 0.9 give sufficiently good results.

It should be noted that in most cases, the load balancing is independent of the above parameters. These attain significance only in case of very complicated geometries.

II.4 EXAMPLES

II.4.1 A Single Rectangular Block

This is the case of a single rectangular block having a regular grid. On this grid, a perfect load balance was obtained for an unbladed block, and satisfactory balance for a bladed block.

II.4.2 Two Adjacent Rectangular Blocks

The next test case considered two adjacent blocks, each of which contains a regular grids. Again, for this simple case, a perfect load balance was obtained for two unbladed blocks.

II.4.3 Grid for General Electric Energy Efficient Engine (GE-EEE)

This test case pertains to the Energy Efficient Engine model developed by General Electric. This model has been used extensively as computational-intensive tests for `ENG10` [35]. The grid was generated using `ENG10` preprocessors [36,37]. It contains 19 original blocks with approximately 115,000 grid points.

The initial load balance is only 15%, as the computational load is heavily dominated by the light-blue block of Figure II.6. This block contains a very fine grid because of the presence of a multistage compressor. A load balancing factor of approximately 80% was finally obtained. Stages of the load-balancing process carried out by `LB` for this fairly complex model are illustrated in color Figures II.6 through II.9.

II.5 CONCLUSIONS

A simple but effective algorithm for load-balancing discretizations consisting of multiple regular-grid blocks has been developed. Preliminary results suggest that the algorithm yields satisfactory results in the test cases considered here. These test cases have included a axisymmetric aerodynamic model of the complete GE-EEE, which has over 10^5 grid points. A load balance of approximately 80% was achieved for this demanding case.

A worthwhile refinement of LB would be the inclusion of *block weights* that account for computational intensity due to the presence of effects such as compression or combustion in specific regions. Such weights might be estimated from CPU measurements on sequential or vector machines, and fed to LB to further improve the decomposition logic.

Acknowledgement

Mr. Udayan Gumaste, who designed and wrote LB, would like to thank Dr. Mark Stewart for his support and assistance during the development of this program. He also acknowledges productive suggestions from Prof. Farhat.

Figure II.6 : Initial Grid for GE–EEE ENG10 Model
(19 blocks, Load Balance : 0.1475)

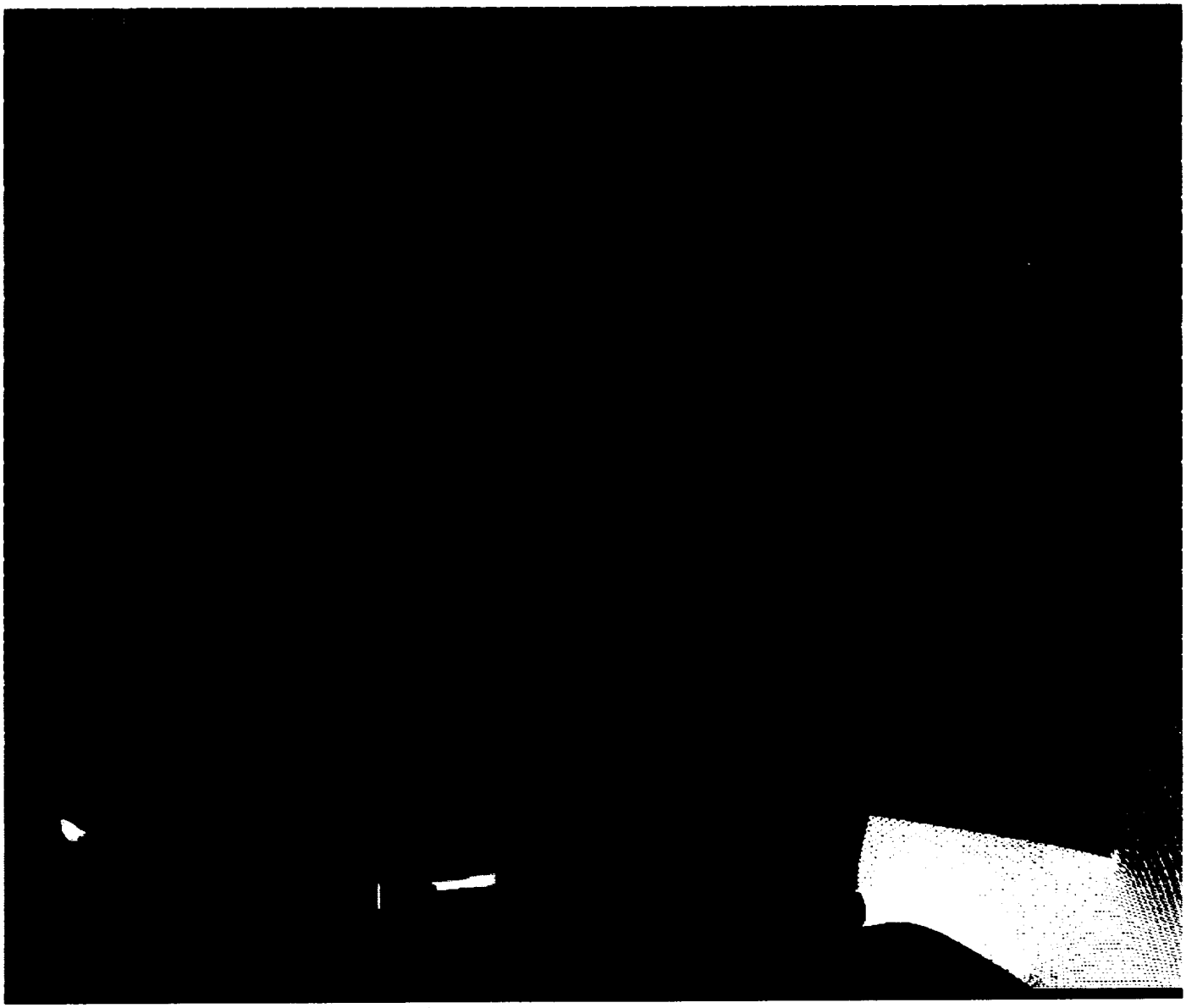

Figure II.7 : Grid for GE–EEE model after Maximum Merging of Adjacent Blocks
(Load Balance : 0.1123)

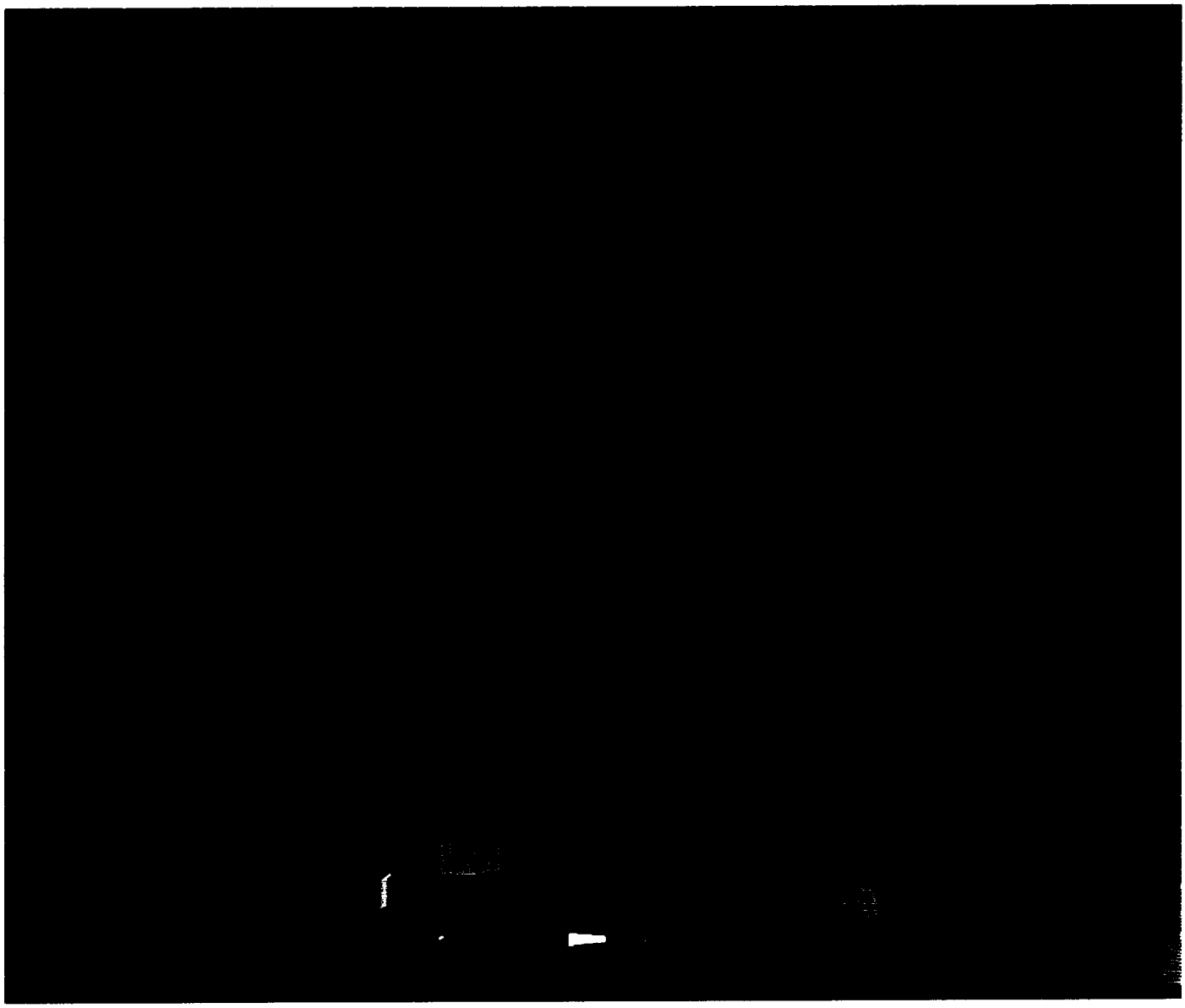

Figure II.8 : Grid for GE–EEE Model after Cutting Large Blocks
(Load Balance : 0.6553)

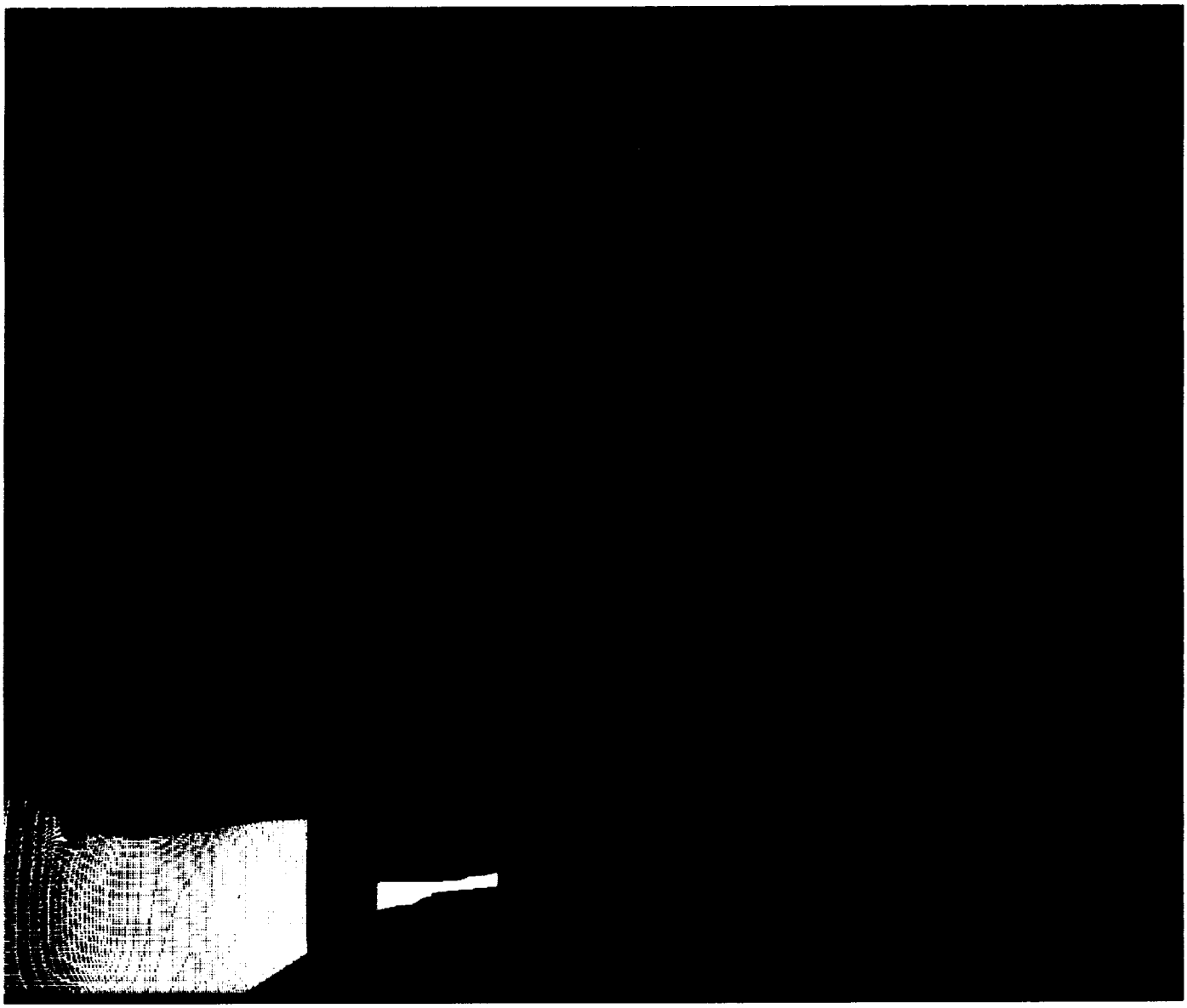

Figure II.9 : Final Configuration of GE–EEE Grid produced by LB
(Load Balance : 0.7943)

REFERENCES

1. W. K. Anderson, J. L. Thomas and C .L. Rumsey, Extension and application of flux-vector splitting to unsteady calculations on dynamic meshes, AIAA Paper No. 87-1152-CP, 1987.

2. E. Barszcz, Intercube communication on the iPSC/860, Scalable High Performance Computing Conference, Williamsburg, April 26-29, 1992.

3. J. T. Batina, Unsteady Euler airfoil solutions using unstructured dynamic meshes, AIAA Paper No. 89-0115, *AIAA 27th Aerospace Sciences Meeting*, Reno, Nevada, January 9–12, 1989.

4. T. Belytschko, P. Smolenski and W. K. Liu, Stability of multi-time step partitioned integrators for first-order finite element systems, *Comput. Meths. Appl. Mech. Engrg.*, **49** (1985) 281–297.

5. M. Blair, M. H. Williams and T. A. Weisshaar, Time domain simulations of a flexible wing in subsonic compressible flow, AIAA Paper No. 90-1153, *AIAA 8th Applied Aerodynamics Conference*, Portland, Oregon, August 20–22, 1990.

6. C. J. Borland and D. P. Rizzetta, Nonlinear transonic flutter analysis, *AIAA Journal*, **20** (1982) 1606–1615.

7. J. Donea, An arbitrary Lagrangian-Eulerian finite element method for transient fluid-structure interactions, *Comput. Meths. Appl. Mech. Engrg.*, **33** (1982) 689–723.

8. C. Farhat and T. Y. Lin, Transient aeroelastic computations using multiple moving frames of reference, AIAA Paper No. 90-3053, *AIAA 8th Applied Aerodynamics Conference*, Portland, Oregon, August 20–22, 1990.

9. C. Farhat, K. C. Park and Y. D. Pelerin, An unconditionally stable staggered algorithm for transient finite element analysis of coupled thermoelastic problems, *Comput. Meths. Appl. Mech. Engrg.*, **85** (1991) 349–365.

10. C. Farhat, S. Lanteri and L. Fezoui, Mixed finite volume/finite element massively parallel computations: Euler flows, unstructured grids, and upwind approximations, in *Unstructured Scientific Computation on Scalable Multiprocessors*, ed. by P. Mehrotra, J. Saltz, and R. Voigt, MIT Press, (1992) 253–283.

11. C. Farhat and T. Y. Lin, A structure attached corotational fluid grid for transient aeroelastic computations, *AIAA Journal*, **31** (1993) 597–599

12. C. Farhat, L. Fezoui, and S. Lanteri, Two-dimensional viscous flow computations on the Connection Machine: unstructured meshes, upwind schemes, and massively parallel computations, *Comput. Meths. Appl. Mech. Engrg.*, **102** (1993) 61–88.

13. C. Farhat and M. Lesoinne, Automatic partitioning of unstructured meshes for the parallel solution of problems in computational mechanics, *Internat. J. Numer. Meths. Engrg.*, **36**, (1993) 745–764.

14. C. Farhat and S. Lanteri, Simulation of compressible viscous flows on a variety of MPPs: computational algorithms for unstructured dynamic meshes and performance results, *Comput. Meths. Appl. Mech. Engrg.*, **119**, (1994) 35–60.

15. C. Farhat, L. Crivelli and F. X. Roux, A transient FETI methodology for large-scale parallel implicit computations in structural mechanics, *Internat. J. Numer. Meths. Engrg.*, **37**, (1994) 1945–1975.

16. C. Farhat, L. Crivelli and F. X. Roux, Extending substructure based iterative solvers to multiple load and repeated analyses, *Comput. Meths. Appl. Mech. Engrg.*, **117** (1994) 195–209.

17. C. Farhat, S. Lanteri and H. D. Simon, TOP/DOMDEC, A software tool for mesh partitioning and parallel processing, *J. Comput. Sys. Engrg.*, in press.

18. C. Farhat, P. S. Chen and P. Stern, Towards the ultimate iterative substructuring method: combined numerical and parallel scalability, and multiple load cases, *J. Comput. Sys. Engrg.*, in press.

19. A. Geist, A. Beguelin, J. Dongarra, R. Mancheck, V. Sunderam, PVM 3.0 User's Guide and Reference Manual, Technical Report ORNL/TM-12187, Oak Ridge National Laboratory, 1993.

20. G. P. Guruswamy, Time-accurate unsteady aerodynamic and aeroelastic calculations of wings using Euler equations, AIAA Paper No. 88-2281, *AIAA 29th Structures, Structural Dynamics and Materials Conference*, Williamsburg, Virginia, April, 18–20, 1988.

21. W. J. Hesse and N. V. S. Mumford, *Jet Propulsion for Aerospace Applications*, 2nd ed., Pitnam Pubs., New York, N.Y., 1964, Chapter 11.

22. O. A. Kandil and H. A. Chuang, Unsteady vortex-dominated flows around maneuvering wings over a wide range of mach numbers, AIAA Paper No. 88-0317,*AIAA 26th Aerospace Sciences Meeting*, Reno, Nevada, January 11–14, 1988.

23. S. Lanteri and C. Farhat, Viscous flow computations on MPP systems: implementational issues and performance results for unstructured grids, in *Parallel Processing for Scientific Computing*, ed. by R. F. Sincovec *et. al.*, SIAM (1993) 65–70.

24. M. Lesoinne and C. Farhat, Stability analysis of dynamic meshes for transient aeroelastic computations, AIAA Paper No. 93-3325, *11th AIAA Computational Fluid Dynamics Conference*, Orlando, Florida, July 6–9, 1993.

25. M. Lesoinne and C. Farhat, Geometric conservation laws for aeroelastic computations Using unstructured dynamic meshes, AIAA Paper No. 95-1709, 1995.

26. M. Loriot, MS3D: Mesh Splitter for 3D Applications, User's Manual.

27. N. Maman and C. Farhat, Matching fluid and structure meshes for aeroelastic computations: a parallel approach, *Computers & Structures*, in press.

28. B. NKonga and H. Guillard, Godunov type method on non-structured meshes for three-dimensional moving boundary problems, *Comput. Meths. Appl. Mech. Engrg.*, **113**, (1994) 183–204.

29. K. C. Park, C. A. Felippa and J. A. DeRuntz, Stabilization of staggered solution procedures for fluid-dtructure interaction analysis, in *Computational Methods for Fluid-Structure Interaction Problems*, ed. by T. Belytschko and T. L. Geers, AMD Vol. 26, American Society of Mechanical Engineers, ASME, New York (1977) 95–124

30. K. C. Park and C. A. Felippa, Partitioned analysis of coupled systems, in: Computational Methods for Transient Analysis, T. Belytschko and T. J. R. Hughes, Eds., North-Holland Pub. Co. (1983) 157–219.

31. S. Piperno and C. Farhat, Partitioned procedures for the transient solution of coupled aeroelastic problems, *Comput. Meths. Appl. Mech. Engrg.*, to appear.

32. E. Pramono and S. K. Weeratunga, Aeroelastic computations for wings through direct coupling on distributed-memory MIMD parallel computers, AIAA Paper No. 94-0095, 32nd Aerospace Sciences Meeting, Reno, January 10–13, 1994.

33. R. D. Rausch, J. T. Batina and T. Y. Yang, Euler flutter analysis of airfoils using unstructured dynamic meshes, AIAA Paper No. 89-13834, 30th Structures, Structural Dynamics and Materials Conference, Mobile, Alabama, April 3–5, 1989.

34. V. Shankar and H. Ide, Aeroelastic computations of flexible configurations, *Computers & Structures*, **30** (1988) 15–28.

35. M. L. Stewart, Axisymmetric aerodynamic numerical analysis of a turbofan engine, Draft paper, NASA Lewis Research Center, May 1994.

36. M. L. Stewart, Description of ENG10 subroutines and related programs, NASA Lewis Research Center, October 1994.

37. M. L. Stewart, A Multiblock Grid Generation Technique Applied to a Jet Engine Configuration, NASA CP-3143, NASA Lewis Research Center, 1992.

38. T. W. Strganac and D. T. Mook, Numerical model of unsteady subsonic aeroelastic behavior, *AIAA Journal*, **28** (1990) 903–909.

39. T. Tezduyar, M. Behr and J. Liou, A new strategy for finite element computations involving moving boundaries and interfaces - The deforming spatial domain/space-time procedure: I. The concept and the preliminary numerical tests, *Comput. Meths. Appl. Mech. Engrg.*, **94** (1992) 339–351.

40. P. D. Thomas and C. K. Lombard, Geometric conservation law and its application to flow computations on moving grids, *AIAA Journal*, **17**, (1979) 1030–1037.

41. B. Van Leer, Towards the ultimate conservative difference scheme V: a second-order sequel to Godunov's method, *J. Comp. Phys.*, **32** (1979).